7

INFLUENCE OF MAGNETIC FIELD ON WATER BASED COMPOSITE NANOFLUID FLOW

Content of this chapter is published in:

International Journal of Applied and Computational Mathematics **(Springer)** 7 (1) (2020), 1-24.

INFLUENCE OF MAGNETIC FIELD ON WATER BASED COMPOSITE NANOFLUID FLOW.

The restriction of the conventional fluids to expedite cooling/heating rates give rise to exploration of nanofluids. Generally, water based single phase nanofluids containing nanoparticles such as CuO or Al2O3 are discussed. Enhancement of heat transfer is beneficial in engineering and actual world problems. To achieve this, experiments considering composite nanoparticles in place of single nanoparticle based nanofluids are performed. Consequently, investigators are fascinated towards heat transfer properties of composite nanofluids. Thermal conductivity of nanofluids is high, which is a motivation in this area, thus many investigators are doing research intensively.

7.1 Introduction of the problem:

Choi and Eastman [130] were probably the first to employ a mixture of nanoparticles and base fluid that such fluidswere designated as “nano-fluids”. Experimental studies have displayed that with 1%–5% volume of solid metallic or metallicoxide particles, the effective thermal conductivity of the resulting mixture can be increased by 20% compared tothat of the base fluid [53]. Nano-fluids exhibit non-Newtonian behavior. Goud et al. [158] discussed evaporation of polystyrene encapsulated phase change composite material based nanofluids whereas Chaudhari et al. [128] studied heat transfer characteristics of Al_2O_3 and CuO nanofluids for machining application. Effect of magnetic field on electrically conducting fluids has many applications in almost all branches of science and engineering such as generators, coolant in huge nuclear power plants, plasma and bearings. Interaction between the electrically conducting fluid and a magnetic field is used as a control mechanism in material manufacturing industry, as the convection currents are suppressed by Lorentz force which is produced by the magnetic field. In pharmaceutical as well as environmental science, MHD has been playing a vital role in the application of fluid dynamics and medical sciences, owing to its implications in chemical fluids as well as metallurgical fields. Research works on MHD have been significantly advanced during the last few years in natural sciences and engineering disciplines after the pioneer work of Hartmann [52] in liquid metal duct flows under the influence of a strong external magnetic field. Lund et al. [60] studied multiple solution of Cu–Al2O3/H2O nanofluid contains hybrid nanomaterials over a shrinking surface.

Radiations due to heat transfer effects on different flows are very important in space technology and high temperature processes. Thermal radiation parameter effects may play an important role in controlling heat transfer in polymer processing industry.

The basic law governing the flow of fluids through porous media is Darcy's Law. Thermophoresis and Brownian motion is important phenomena in heat and mass transfer fluid flow problems. Recently, Patel and Singh [33] studied thermophoresis and brownian motion effects on mixed convection MHD micropolar fluid flow due to nonlinear stretched sheet in porous medium. Mittal and Patel [6] studied influence of thermophoresis and Brownian motion on mixed convection two dimensional MHD Casson fluid flow with non-linear radiation and heat generation whereas Mittal and Kataria [5] considered three dimensional CuO–Water nanofluid flow with Brownian motion and thermal radiation.

7.2 Novelty of the Problem:

The works stated that no effort is made to study the effects of thermal radiation and Brownian motion on MHD flow water based composite nanofluid passing through a porous medium. So, the objective of present study to be develop the mathematical modeling for Brownian motion effects on MHD flow water based composite nanofluid with thermal radiation. We consider the fluid flow past in porous medium. HAM Method applied for finding the solution of governing equations. Skin friction, Nusselt number and Sherwood number are obtained and presented in graphical form.

7.3 Mathematical Formulation of the Problem:

It is assumed that hybrid nanofluid (Mixture of Al_2O_3 – CuO - Water nanofluid) "flows between two horizontal parallel plates placed L units apart through a porous medium. A coordinate system (x, y, z) is such that origin is at the lower plate as shown in Figure 7.1. The lower plate is stretched by two equal forces in opposite directions. The plates along with the fluid rotate about y axis with angular velocity Ω. A uniform magnetic flux with density B_0 is applied along $y - axis$. Under these assumptions, governing equations are:"

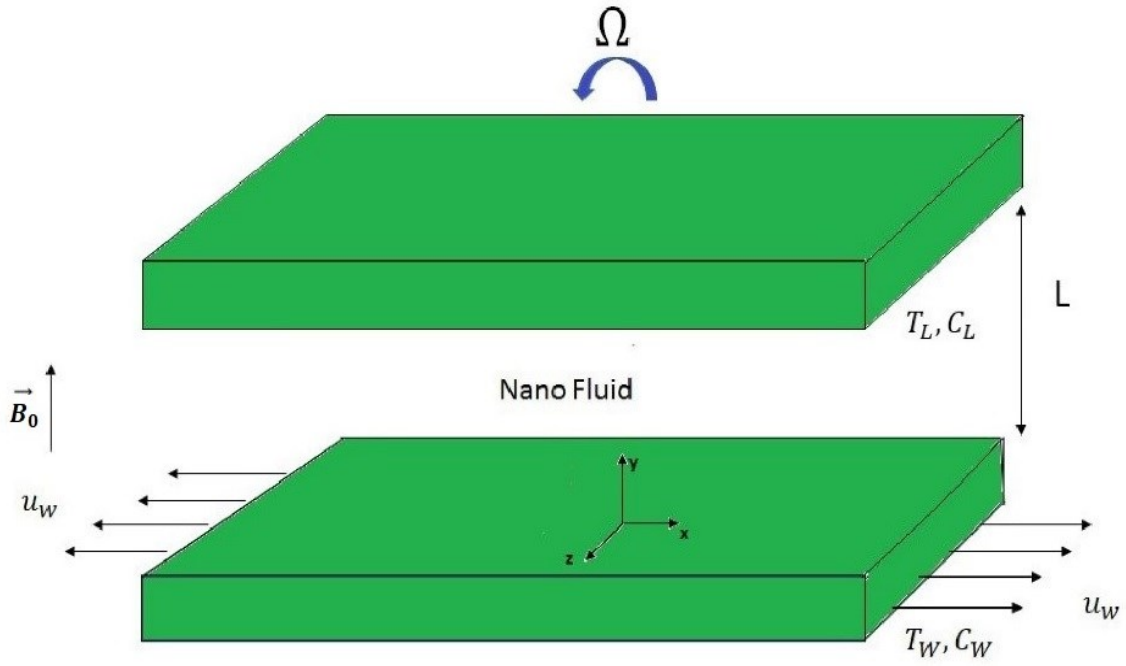

Figure 7.1: Physical sketch of the problem.

$$\frac{\partial u'}{\partial x}+\frac{\partial v'}{\partial y}+\frac{\partial w'}{\partial z}=0 \tag{7.1}$$

$$\rho_{hnf}\left(u'\frac{\partial u'}{\partial x}+v'\frac{\partial u'}{\partial y}+2\Omega w'\right)=\mu_{hnf}\left(\frac{\partial^2 u'}{\partial x^2}+\frac{\partial^2 u'}{\partial y^2}\right)-\sigma_{hnf}{B_0}^2u'-\frac{\mu_{hnf}\emptyset}{{k_1}'}u' \tag{7.2}$$

$$\rho_{hnf}\left(v'\frac{\partial v'}{\partial y}\right)=\mu_{hnf}\left(\frac{\partial^2 v'}{\partial x^2}+\frac{\partial^2 v'}{\partial y^2}\right) \tag{7.3}$$

$$\rho_{hnf}\left(u'\frac{\partial w'}{\partial x}+v'\frac{\partial w'}{\partial y}-2\Omega w'\right)=\mu_{hnf}\left(\frac{\partial^2 w'}{\partial x^2}+\frac{\partial^2 w'}{\partial y^2}\right)-\sigma_{hnf}{B_0}^2w'-\frac{\mu_{hnf}\emptyset}{{k_1}'}w' \tag{7.4}$$

$$\left(\rho c_p\right)_{hnf}\left(u'\frac{\partial T'}{\partial x}+v'\frac{\partial T'}{\partial y}+w'\frac{\partial T'}{\partial z}\right)=k_{nf}\left(\frac{\partial^2 T'}{\partial x^2}+\frac{\partial^2 T'}{\partial y^2}+\frac{\partial^2 T'}{\partial z^2}\right)+\mu_{hnf}\left(\frac{D_T}{T_w}\left(\left(\frac{\partial T'}{\partial x}\right)^2+\left(\frac{\partial T'}{\partial y}\right)^2+\left(\frac{\partial T'}{\partial z}\right)^2\right)+D_B\left(\frac{\partial C}{\partial x}\frac{\partial T'}{\partial x}+\frac{\partial C}{\partial y}\frac{\partial T'}{\partial y}+\frac{\partial C}{\partial z}\frac{\partial T'}{\partial z}\right)\right)-\frac{\partial q_r}{\partial y} \tag{7.5}$$

$$u'\frac{\partial C}{\partial x}+v'\frac{\partial C}{\partial y}+w'\frac{\partial C}{\partial z}=D_B\left(\frac{\partial^2 C}{\partial x^2}+\frac{\partial^2 C}{\partial y^2}+\frac{\partial^2 C}{\partial z^2}\right)+\frac{D_T}{T_w}\left(\frac{\partial^2 T'}{\partial x^2}+\frac{\partial^2 T'}{\partial y^2}+\frac{\partial^2 T'}{\partial z^2}\right) \tag{7.6}$$

From Ref. [5] and [37], we write

$$\rho_{hnf} = \{(1-\varphi_2)[(1-\varphi_1)\rho_{bf} + \varphi_1\rho_{s1}]\} + \varphi_2\rho_{s2} \quad (7.7)$$

$$\frac{\sigma_{hnf}}{\sigma_{bf}} = \frac{\sigma_{S_2}+2\sigma_{bf}-2\varphi_2(\sigma_{bf}-\sigma_{S_2})}{\sigma_{S_2}+2\sigma_{bf}+\varphi_2(\sigma_{bf}-\sigma_{S_2})}, \quad (7.8)$$

$$\frac{\sigma_{bf}}{\sigma_f} = \frac{\sigma_{S_1}+2\sigma_f-2\varphi_1(\sigma_f-\sigma_{S_1})}{\sigma_{S_1}+2\sigma_f+\varphi_1(\sigma_f-\sigma_{S_1})} \quad (7.9)$$

$$(\rho c_p)_{hnf} = \left\{(1-\varphi_2)\left[(1-\varphi_1)(\rho c_p)_f + \varphi_1(\rho c_p)_{s1}\right]\right\} + \varphi_2(\rho c_p)_{s2} \quad (7.10)$$

$$\frac{k_{hnf}}{k_{bf}} = \frac{k_{S_2}+(n-1)k_{bf}-(n-1)\varphi_2(k_{bf}-k_{S_2})}{k_{S_2}+(n-1)k_{bf}+\varphi_2(k_{bf}-k_{S_2})}, \quad (7.11)$$

Where

$$\frac{k_{bf}}{k_f} = \frac{k_{S_1}+(n-1)k_f-(n-1)\varphi_1(k_f-k_{S_1})}{k_{S_1}+(n-1)k_f+\varphi_1(k_f-k_{S_1})}, \quad (7.12)$$

$$\mu_{hnf} = \frac{\mu_{bf}}{(1-\varphi_1)^{2.5}(1-\varphi_2)^{2.5}} \quad (7.13)$$

Table 1 demonstrates values of thermo-physical properties for water as base fluid and different materials used as suspended particles.

Table 7.1: Thermo-physical properties of water and nanoparticles.

Physical properties	Fluid phase (water)	Copper	Alumina	Silver
$C_p(J/(KgK))$	4179	385	765	235
$\rho(Kg/m^3)$	997.1	8933	3970	10500
$k(W/(mK))$	0.613	401	40	429
$\beta \times 10^{-5}(K^{-1})$	21	1.67	0.85	1.89
$\sigma((\Omega m)^{-1})$	0.05	$5.96*10^7$	10^{-10}	$3.60*10^7$

q_r [127] can be expressed as,

$$q_r = -\frac{4\sigma^*}{3k^*}\frac{\partial T^4}{\partial y} = -\frac{4\sigma^*}{3k^*}\frac{\partial(4T_0{}^3T-3T_0{}^4)}{\partial y} \quad (7.14)$$

"Subject to boundary conditions"

$$u' = ax;\ v' = 0;\ w' = 0;\ T' = T_w\ at\ y = 0 \quad (7.15)$$

$$u' = 0;\ v' = 0;\ w' = 0;\ T' = T_L\ at\ y = L \tag{7.16}$$

"Introducing non dimensional variables"

$$\eta = \frac{y}{L},\ u' = axf'(\eta), v' = -ahf(\eta),\ w' = axg(\eta),\ \theta(\eta) = \frac{\mathrm{T}\prime - T_L}{T_w - T_L},\ \mathrm{C}(\eta) = \frac{\mathrm{C} - C_L}{C_w - C_L} \tag{7.17}$$

"Therefore dimensionless form of governing equations is given by:"

$$a_1 f^{iv} - Re(f'f'' - ff''') - 2\,R_k\,g' - \left(a_3 M^2 + \frac{a_1}{k_1}\right) f'' = 0 \tag{7.18}$$

$$a_1 g'' - Re(f'g - fg') + 2\,R_k\,f' - \left(a_3 M^2 + \frac{a_1}{k_1}\right) g = 0 \tag{7.19}$$

$$\theta'' + PrRea_2 f\theta' + NbC'\theta' + Nt\theta'^2 = 0 \tag{7.20}$$

$$Nb\mathrm{C}'' + Nt\theta'' + NbReScfC' = 0 \tag{7.21}$$

"Subject to"

$$f = 0, f' = 1, g = 0, \theta = 1,\ C = 1\ at\ \eta = 0$$

$$f = 0, f' = 0, g = 0, \theta = 0,\ \mathrm{C} = 0\ at\ \eta = 1 \tag{7.22}$$

Where,

$$Pr = \frac{\mu_{bf}\,(c_p)_{bf}}{k_{bf}},\ Sc = \frac{\mu_{bf}}{\rho_{bf} D},\ M^2 = \frac{\sigma_{bf} {B_0}^2 L^2}{\rho_{bf} v_{bf}},\ \frac{1}{k_1} = \frac{v\phi^2}{{k_1}' v_{bf}},\ Kr = \frac{\Omega L^2}{v_{bf}}, Re = \frac{aL^2}{v_{bf}},$$

$$Ec = \frac{(aL)^2}{(c_p)_{bf}(\theta_0 - \theta_L)},\ \alpha = \frac{k_{hnf}}{(\rho c_p)_{hnf}},\ Nb = \frac{\left\{(1-\varphi_2)\left[(1-\varphi_1)(\rho c_p)_{bf} + \varphi_1 (\rho c_p)_{s1}\right]\right\} + \varphi_2 (\rho c_p)_{s2}\, D_B C_L}{(\rho c_p)_{bf}\alpha},$$

$$Nt = \frac{\left\{(1-\varphi_2)\left[(1-\varphi_1)(\rho c_p)_{bf} + \varphi_1 (\rho c_p)_{s1}\right]\right\} + \varphi_2 (\rho c_p)_{s2}\, D_B T_L}{(\rho c_p)_{bf}\alpha T_w} \tag{7.23}$$

$$b_0 = (1-\varphi_1)(1-\varphi_2) \tag{7.24}$$

$$b_1 = \left(b_0 + (1-\varphi_2)\varphi_1 \frac{\rho_{s1}}{\rho_f} + \varphi_2 \frac{\rho_{s2}}{\rho_f}\right) \tag{7.25}$$

$$b_2 = \frac{1}{{b_0}^{2.5}} \tag{7.26}$$

$$b_3 = \left(b_0 + (1-\varphi_2)\varphi_1 \frac{(\rho)_{s1}(c_p)_{s1}}{(\rho)_{bf}(c_p)_{bf}} + \varphi_2 \frac{(\rho)_{s2}(c_p)_{s2}}{(\rho)_{bf}(c_p)_{bf}}\right) \quad (7.27)$$

$$b_4 = \frac{k_{hnf}}{k_{bf}} \quad (7.28)$$

$$b_5 = \frac{\sigma_{hnf}}{\sigma_{bf}} \quad (7.29)$$

$$a_1 = \frac{1}{{b_0}^{2.5} b_1} \quad (7.30)$$

$$a_2 = \frac{b_3}{b_4 + R} \quad (7.31)$$

$$a_3 = \frac{b_5}{b_1} \quad (7.32)$$

$$a_4 = \frac{b_2}{b_4} \quad (7.33)$$

$$R = \frac{16\sigma^* {T_0}^3}{3k^* k_{bf}} \quad (7.34)$$

7.4 Solution of the Problem:

Equations (7.18) – (7.21) subject to (7.22) are solved by HAM [122].

Initial guess is given by:

$f_0(\eta) = \frac{-2}{e^2-4e+3} + \frac{e-1}{e-3}\eta + \frac{2-e}{e^2-4e+3}e^{\eta} + \frac{e}{e^2-4e+3}e^{-\eta}$; $g_0(\eta) = 0$; $\theta_0(\eta) = 1-\eta$; $C_0(\eta) = 1-\eta$; (7.35)

with auxiliary linear operators:

$$L_f = \frac{\partial^4 f}{\partial \eta^4} - \frac{\partial^2 f}{\partial \eta^2}\ ,\ L_g = \frac{\partial^2 g}{\partial \eta^2} - \frac{\partial g}{\partial \eta}\ ,\ L_\theta = \frac{\partial^2 \theta}{\partial \eta^2}\ ,\ L_C = \frac{\partial^2 \mathrm{C}}{\partial \eta^2} \quad (7.36)$$

Satisfying

$L_f(C_1 + C_2\,\eta + C_3 e^{\eta} + C_4 e^{-\eta}) = 0,\ L_g(C_5 + C_6 e^{\eta}) = 0,\ L_\theta(C_7 + C_8\eta),\ L_C(C_9 + C_{10}\eta) = 0.$ (7.37)

where $c_1,\ \ c_2, \ldots, c_{10}$ "are the arbitrary constants.

The zero[th] order deformation problems are constructed as follows:

$$(1-p)L_f\left[\hat{f}(\eta;\ p)-f_0(\eta)\right]=p\hbar_f N_f\left[\hat{f}(\eta;\ p),\hat{g}(\eta;\ p),\hat{\theta}(\eta;\ p),\hat{C}(\eta;\ p)\right] \tag{7.38}$$

$$(1-p)L_g[\hat{g}(\eta;\ p)-g_0(\eta)]=p\hbar_g N_g\left[\hat{f}(\eta;\ p),\hat{g}(\eta;\ p),\hat{\theta}(\eta;\ p),\hat{C}(\eta;\ p)\right] \tag{7.39}$$

$$(1-p)L_\theta\left[\hat{\theta}(\eta;\ p)-\theta_0(\eta)\right]=p\hbar_\theta N_\theta\left[\hat{f}(\eta;\ p),\hat{g}(\eta;\ p),\hat{\theta}(\eta;\ p),\hat{C}(\eta;\ p)\right] \tag{7.40}$$

$$(1-p)L_C\left[\hat{C}(\eta;\ p)-C_0(\eta)\right]=p\hbar_C N_C\left[\hat{f}(\eta;\ p),\hat{g}(\eta;\ p),\hat{\theta}(\eta;\ p),\hat{C}(\eta;\ p)\right] \tag{7.41}$$

Subject to:

$$\hat{f}(0;\ p)=0,\quad \hat{f}'(0;\ p)=1; \tag{7.42}$$

$$\hat{f}(1;\ p)=0,\quad \hat{f}'(1;\ p)=0; \tag{7.43}$$

$$\hat{g}(0;\ p)=0,\quad \hat{g}(1;\ p)=0; \tag{7.44}$$

$$\hat{\theta}(0;\ p)=1,\quad \hat{\theta}(1;\ p)=0; \tag{7.45}$$

$$\hat{C}(0;\ p)=1,\quad \hat{C}(1;\ p)=0. \tag{7.46}$$

The nonlinear operators are given by

$$N_f\left[\hat{f}(\eta;\ p),\hat{g}(\eta;\ p),\hat{\theta}(\eta;\ p),\hat{C}(\eta;\ p)\right]=\ a_1\frac{\partial^4\hat{f}}{\partial\eta^4}-Re\left(\frac{\partial\hat{f}}{\partial\eta}\frac{\partial^2\hat{f}}{\partial\eta^2}-\hat{f}\frac{\partial^3\hat{f}}{\partial\eta^3}\right)-2\,R_k\,\frac{\partial\hat{g}}{\partial\eta}-\left(a_3M^2+\frac{a_1}{k_1}\right)\frac{\partial^2\hat{f}}{\partial\eta^2} \tag{7.47}$$

$$N_g\left[\hat{f}(\eta;\ p),\hat{g}(\eta;\ p),\hat{\theta}(\eta;\ p),\hat{C}(\eta;\ p)\right]=a_1\frac{\partial^2\hat{g}}{\partial\eta^2}-Re\left(g\,\frac{\partial\hat{f}}{\partial\eta}-f\,\frac{\partial\hat{g}}{\partial\eta}\right)+2\,R_k\,\frac{\partial\hat{f}}{\partial\eta}-\left(a_3M^2+\frac{a_1}{k_1}\right) \tag{7.48}$$

$$N_\theta\left[\hat{f}(\eta;\ p),\hat{g}(\eta;\ p),\hat{\theta}(\eta;\ p),\hat{C}(\eta;\ p)\right]=\ \frac{\partial^2\hat{\theta}}{\partial\eta^2}+PrRea_2\hat{f}\frac{\partial\hat{\theta}}{\partial\eta}+Nb\frac{\partial\hat{C}}{\partial\eta}\frac{\partial\hat{\theta}}{\partial\eta}+Nt\left(\frac{\partial\hat{\theta}}{\partial\eta}\right)^2 \tag{7.49}$$

$$N_C\left[\hat{f}(\eta;\ p), \hat{g}(\eta;\ p), \hat{\theta}(\eta;\ p), \hat{C}(\eta;\ p)\right] = \quad Nb\frac{\partial^2 \hat{C}}{\partial \eta^2} + Nt\frac{\partial^2 \hat{\theta}}{\partial \eta^2} + Nb\ Re\ Sc\ \hat{f}\frac{\partial \hat{C}}{\partial \eta} \tag{7.50}$$

Where $\hat{f}(\eta;\ p), \hat{g}(\eta;\ p), \hat{\theta}(\eta;\ p)$ and $\hat{C}(\eta;\ p)$ are unknown functions with respect to η and p. $\hbar_f, \hbar_g, \hbar_\theta$ and $\hbar_C$ are the non-zero auxiliary parameters and N_f, N_g, N_θ and N_C are the nonlinear operators.

Also $p \in (0,\ 1)$ is an embedding parameter. For $p = 0$ and $p = 1$ we have

$$\hat{f}(\eta; 0) = f_0(\eta), \hat{f}(\eta; 1) = f(\eta), \tag{7.51}$$

$$\hat{g}(\eta; 0) = g_0(\eta), \hat{g}(\eta; 1) = g(\eta), \tag{7.52}$$

$$\hat{\theta}(\eta; 0) = \theta_0(\eta), \hat{\theta}(\eta; 1) = \theta(\eta), \tag{7.53}$$

$$\hat{\mathrm{C}}(\eta; 0) = C_0(\eta), \hat{C}(\eta; 1) = \mathrm{C}(\eta). \tag{7.54}$$

When p varies from 0 to 1, then $\hat{f}, \hat{g}, \hat{\theta}$ and $\hat{C}$ vary from $f_0,\ g_0, \theta_0$ and C_0 to f, g, θ and C. Taylor's series expansion yields:

$$\hat{f}(\eta;\ p) = f_0(\eta) + \sum_{m=1}^{\infty} f_m(\eta)p^m, \tag{7.55}$$

$$\hat{g}(\eta;\ p) = g_0(\eta) + \sum_{m=1}^{\infty} g_m(\eta)p^m, \tag{7.56}$$

$$\hat{\theta}(\eta;\ p) = \theta_0(\eta) + \sum_{m=1}^{\infty} \theta_m(\eta)p^m, \tag{7.57}$$

$$\hat{\mathrm{C}}(\eta;\ p) = \mathrm{C}_0(\eta) + \sum_{m=1}^{\infty} \mathrm{C}_m(\eta)p^m. \tag{7.58}$$

Where

$$f_m(\eta) = \frac{1}{m!}\left[\frac{\partial^m f(\eta; p)}{\partial p^m}\right]_{p=0}, \tag{7.59}$$

$$g_m(\eta) = \frac{1}{m!}\left[\frac{\partial^m g(\eta; p)}{\partial p^m}\right]_{p=0}, \tag{7.60}$$

$$\theta_m(\eta) = \frac{1}{m!}\left[\frac{\partial^m \theta(\eta; p)}{\partial p^m}\right]_{p=0}, \tag{7.61}$$

$$C_m(\eta) = \frac{1}{m!}\left[\frac{\partial^m \mathrm{C}(\eta; p)}{\partial p^m}\right]_{p=0}. \tag{7.62}$$

$\hbar_f, \hbar_g, \hbar_\theta$ and $\hbar_C$ are chosen such that Equations (7.35) to (7.37) converge when $p = 1$, Hence,

"$f(\eta) = f_0(\eta) + \sum_{m=1}^{\infty} f_m(\eta)$, (7.63)

$g(\eta) = g_0(\eta) + \sum_{m=1}^{\infty} g_m(\eta)$, (7.64)

$\theta(\eta) = \theta_0(\eta) + \sum_{m=1}^{\infty} \theta_m(\eta)$, (7.65)

$\mathrm{C}(\eta) = \mathrm{C}_0(\eta) + \sum_{m=1}^{\infty} \mathrm{C}_m(\eta)$. (7.66)

Differentiating (7.37) – (7.39) and (7.40) – (7.43) m times w.r.t. p and putting $p = 0$, m^{th} order deformation $(m \geq 1)$ can be expressed as"

$L_f[f_m(\eta) - \chi_m f_{m-1}(\eta)] = \hbar_f R_{f,m}(\eta)$, (7.67)

$L_g[g_m(\eta) - \chi_m g_{m-1}(\eta)] = \hbar_g R_{g,m}(\eta)$, (7.68)

$L_\theta[\theta_m(\eta) - \chi_m \theta_{m-1}(\eta)] = \hbar_\theta R_{\theta,m}(\eta)$, (7.69)

$L_{\mathrm{C}}[C_m(\eta) - \chi_m C_{m-1}(\eta)] = \hbar_{\mathrm{C}} R_{\mathrm{C},m}(\eta)$. (7.70)

"Subject to the boundary conditions"

$f_m(0) = f_m'(0) = 0$, (7.71)

$f_m(1) = f_m'(1) = 0$, (7.72)

$g_m(0) = g_m(1) = 0$, (7.73)

$\theta_m(0) = \theta_m(1) = 0$, (7.74)

$\mathrm{C}_m(0) = \mathrm{C}_m(1) = 0$. (7.75)

$$R_{f,m}(\eta) = a_1 f_{m-1}^{iv} - Re\left(\sum_{j=0}^{m-1} f_j' f_{m-1-j}'' - \sum_{j=0}^{m-1} f_j f_{m-1-j}'''\right) - 2\,R_k g_{m-1}' - \left(a_3 M^2 + \frac{a_1}{k_1}\right) f_{m-1}'' \quad (7.76)$$

$$R_{g,m}(\eta) = a_1 g_{m-1}'' - Re\left(\sum_{j=0}^{m-1} f_j'\, g_{m-1-j} - \sum_{j=0}^{m-1} f_j g_{m-1-j}'\right) + 2\,R_k f_{m-1}' - \left(a_3 M^2 + \frac{a_1}{k_1}\right) g_{m-1} \quad (7.77)$$

$$R_{\theta,m}(\eta) = \theta''_{m-1} + PrRea_2 \sum_{j=0}^{m-1} f_j \theta'_{m-1-j} + Nb \sum_{j=0}^{m-1} C'_j \theta'_{m-1-j} + Nt \sum_{j=0}^{m-1} \theta'_j \theta'_{m-1-j} \quad (7.78)$$

$$R_{C,m}(\eta) = NbC''_{m-1} + Nt\theta''_{m-1} + NbReSc \sum_{j=0}^{m-1} f_j C'_{m-1-j} \quad (7.79)$$

"with $\chi_m = \begin{cases} 0, & m \leq 1 \\ 1, & m \geq 1 \end{cases}$, (7.80)

Solving the corresponding m^{th}-order deformation equations,"

$$f_m(\eta) = f_m^*(\eta) + C_1 + C_2\,\eta + C_3 e^{\eta} + C_4 e^{-\eta} \quad (7.81)$$

$$g_m(\eta) = g_m^*(\eta) + C_5 + C_6 e^{\eta} \quad (7.82)$$

$$\theta_m(\eta) = \theta_m^*(\eta) + C_7 + C_8\eta \quad (7.83)$$

$$C_m(\eta) = C_m^*(\eta) + C_9 + C_{10}\eta \quad (7.84)$$

Here f_m^*, g_m^*, θ_m^* *and* C_m^* are particular solutions of mth-order equations and $C_i (\, i = 1,2, \ldots, 10)$ are determined by boundary conditions.

7.4.1 Convergence of Homotopy Solution

Auxiliary parameters $\hbar_f, \hbar_g, \hbar_\theta$ and $\hbar_C$ guarantee convergence of solutions and are obtained in Figures 7.2 – 7.5.

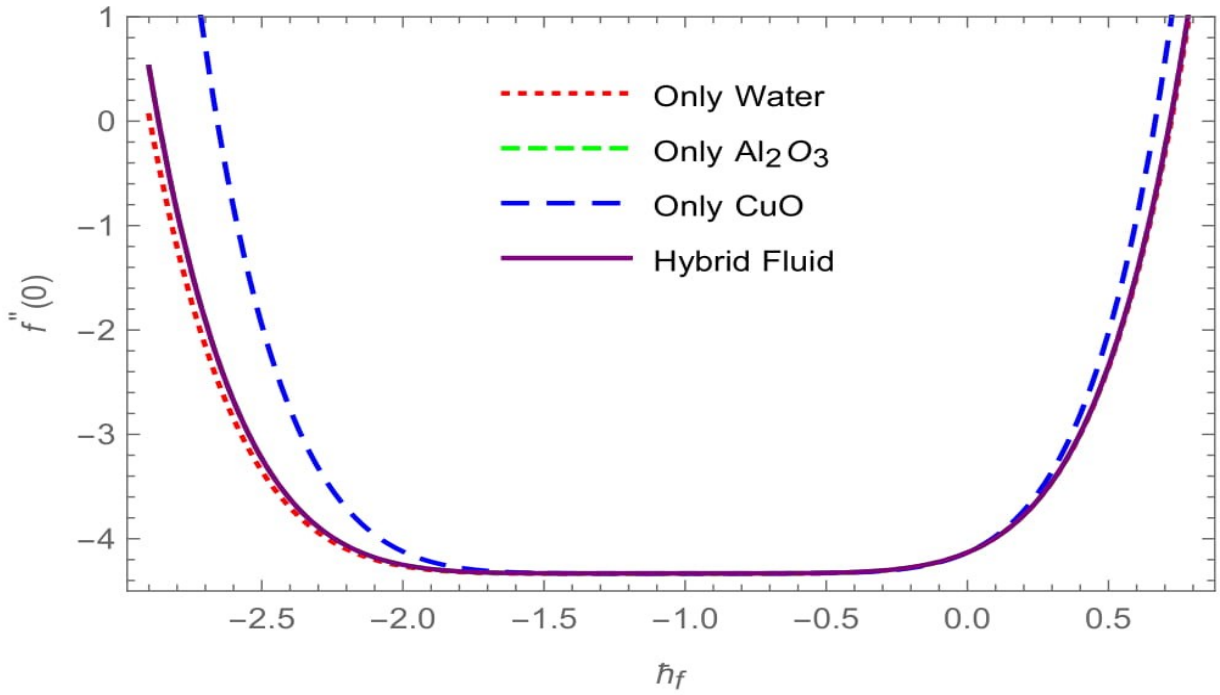

Figure 7.2: h -curve of $f''(\eta)$

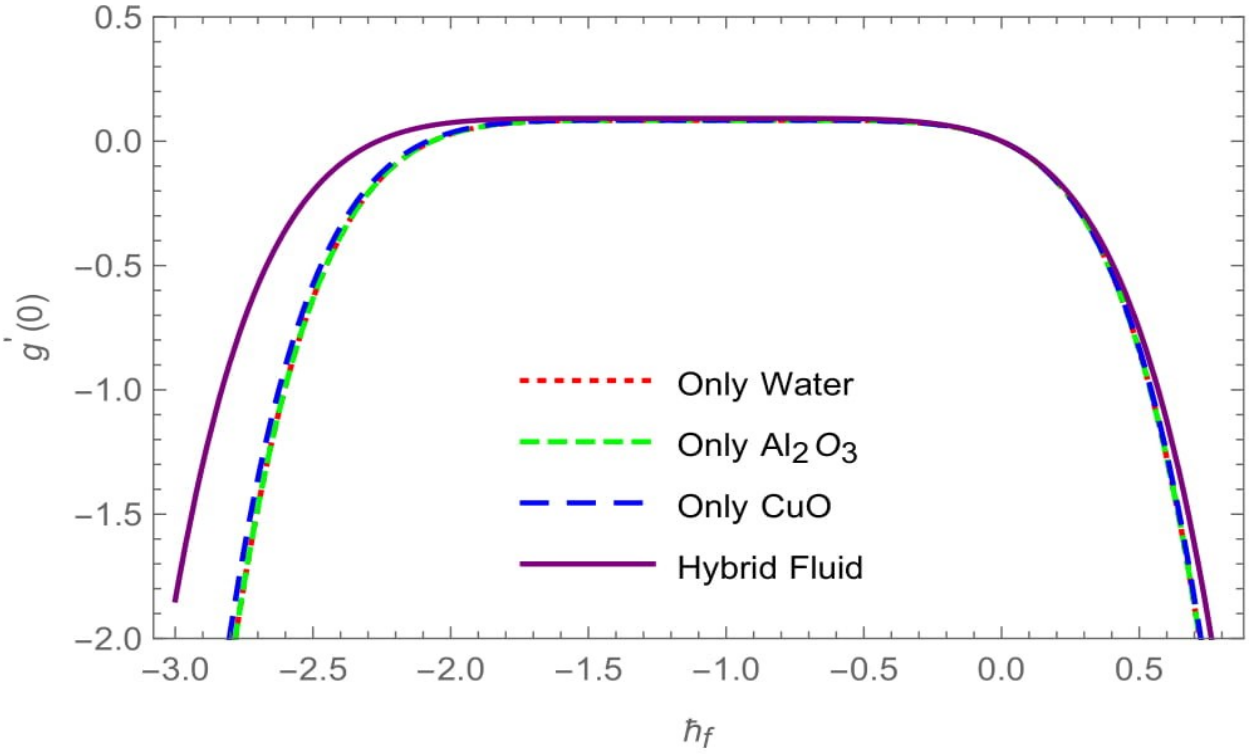

Figure 7.3: h-curve of $g'(\eta)$

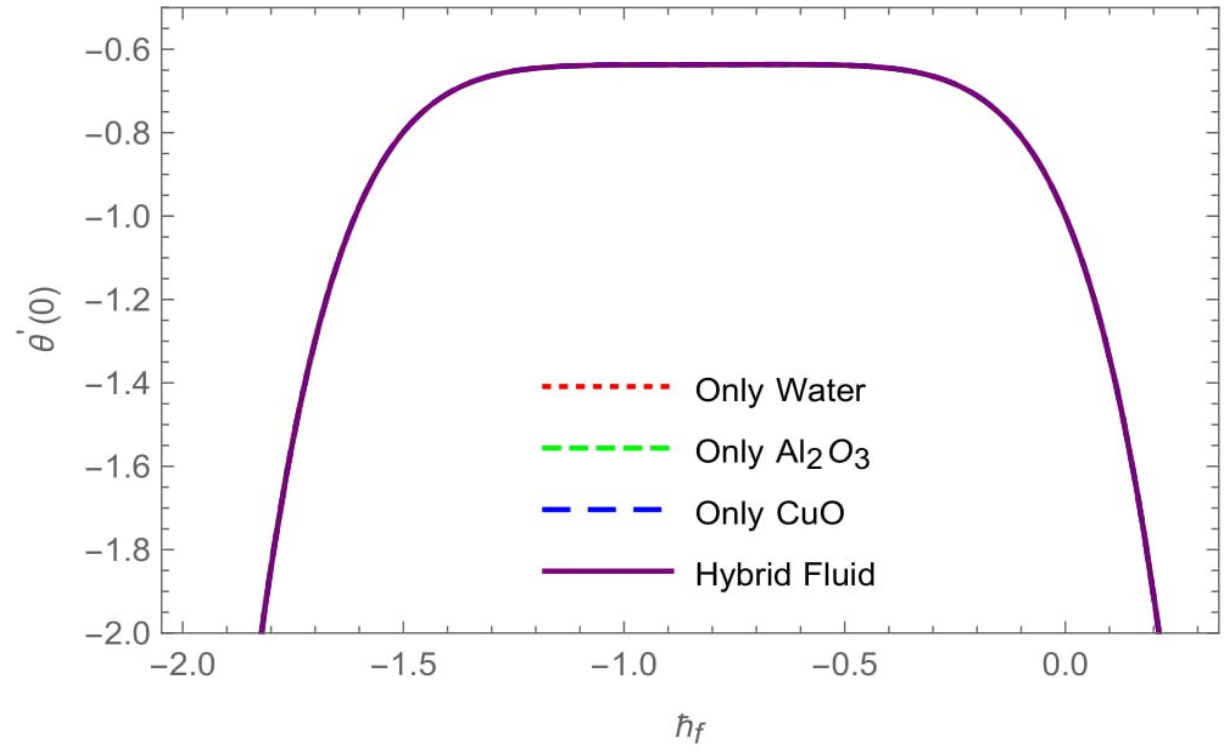

Figure 7.4: h-curve of $\theta'(\eta)$

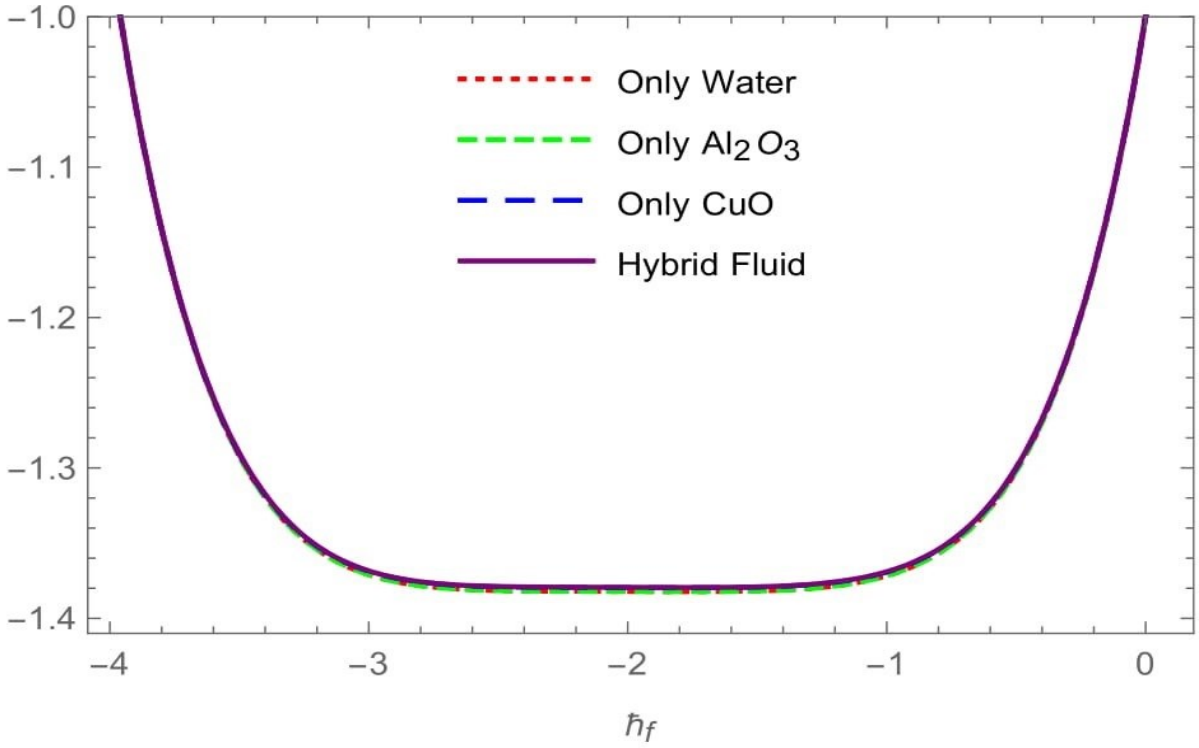

Figure 7.5: h-curve of $C'(\eta)$

7.5 Results and Discussion:

In order to get a clear insight on the physical of the problem, a parametric study is performed and obtained numerical results are clarified with the help of graphical representations. We have presented the velocity, temperature and concentration profiles for different values of physical parameters in Figures 7.6 to 7.37. Figures 7.6 to 7.8 reflects permeability parameter's effects on f, f' and g. It is evident that f and f' have positive correlation with k_1, whereas g has reverse tendency. Due to the effects of porosity, it is obvious to improvement of motion of the fluid. This occurrences is obviously satisfied which is clarifies the physical state that as k_1 increases. Physically, if we increase values of k_1, porosity will increase therefore motion of the fluid also increases. Causes existence of the porous medium in the flow furnishes confrontation to flow. Consequently, the result resistive force tends to sluggish the motion of the fluid along the surface of the plate. Effect of magnetic parameter on velocity profiles f and f' are shown in figures 7.9 to 7.11. From Figure 7.9 and 7.10, it is seen that the velocity profiles as well as the boundary layer thickness decreases when M is increased. The application of a transverse magnetic field results in a resistive type force (called Lorentz force) similar to the drag force, and upon increasing the values of M, the drag force increases which leads to the deaccelerate of the flow. Figure 7.11 illustrate

the influence of magnetic field effects on g. It is depicted that, Magnetic field tends to improve velocity profiles g. Figure 7.12 to 7.14 shows effects of rotation parameter on velocity profiles f, f' and g. From figure 7.12 to 7.13, the rotation parameter R_k tends to reduced velocity in both directions f and f'. This is justifying because Coriolis force, created due to rotation, tends to overturn fluid flow in flow direction in the flow-field. From figure 7.14, it is concluded that the velocity profiles g increase in interval [0, 0.2] after that velocity decrease in interval [0.2, 1]. Figure 7.15 and Figure 7.16 reflects effects of Brownian motion parameter Nb on temperature and concentration profiles. It is evident that, temperature have positive changes whereas concentration have negative changes with increase in Nb. Figures 7.17 and 7.18 shows effects of thermal radiation on temperature and concentration profiles. It is observed that increasing radiation will increase temperature but, concentration has reverse effect. Physically, Due to increasing thermal radiation parameter R, heat is generated in fluid flow, which leads to improvement in heat transfer as well as momentum throughout the fluid flow region. The thermophoresis parameter effects on temperature and concentration profiles are shown in figures 7.19 and 7.20. It is depicted that, heat transfer process increase with increase in Nt whereas concentration decrease with increase in Nt. Figures 7.21 to 7.22 reveals the effects of nanoparticles volume fraction on temperature and concentration. Concentration will increase by increasing volume fraction and temperature will decrease. Figure 7.23 and Figure 7.24 exhibits the temperature and concentration profiles for different values of Prandtl number Pr. It is observed that heat transfer process decreases with increase in Prandtl number Pr whereas mass transfer increases with increase in Pr. It is justified due to the fact that thermal conductivity of the fluid decrease with increase in Prandtl number Pr and hence decrease the thermal boundary layer thickness. Figure 7.25 and 7.26 shows the effects of Schmidt number on temperature and concentration profiles. It is seen that, Schmidt number can decrease temperature and concentration marginally.

Figure 7.27 to 7.37 shows skin friction, Nusselt number and Sherwood number with different physical parameter. It is observed that the skin friction decrease with increase in k_1 whereas increase with R_k. It is also seen that φ Nanoparticle volume fraction increase initially and the decrease with increase in skin friction. It also conclude that Nusselt number decrease with Nb, R, and Nt increase and nusselt number increase with φ increase. It is also observed that Sherwood number decrease with increase in R_k, Nt and Sc and Sherwood number increase with increase in Nb.

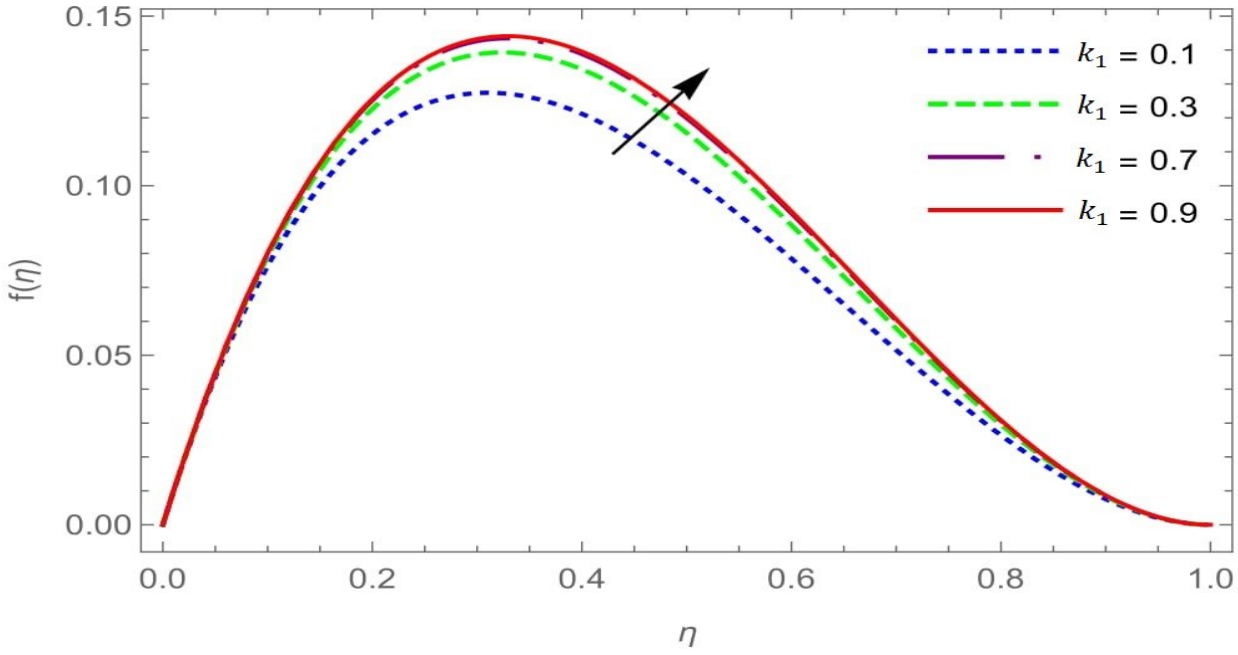

Figure 7.6: $\boldsymbol{f(\eta)}$ for different values of $\boldsymbol{k_1}$.

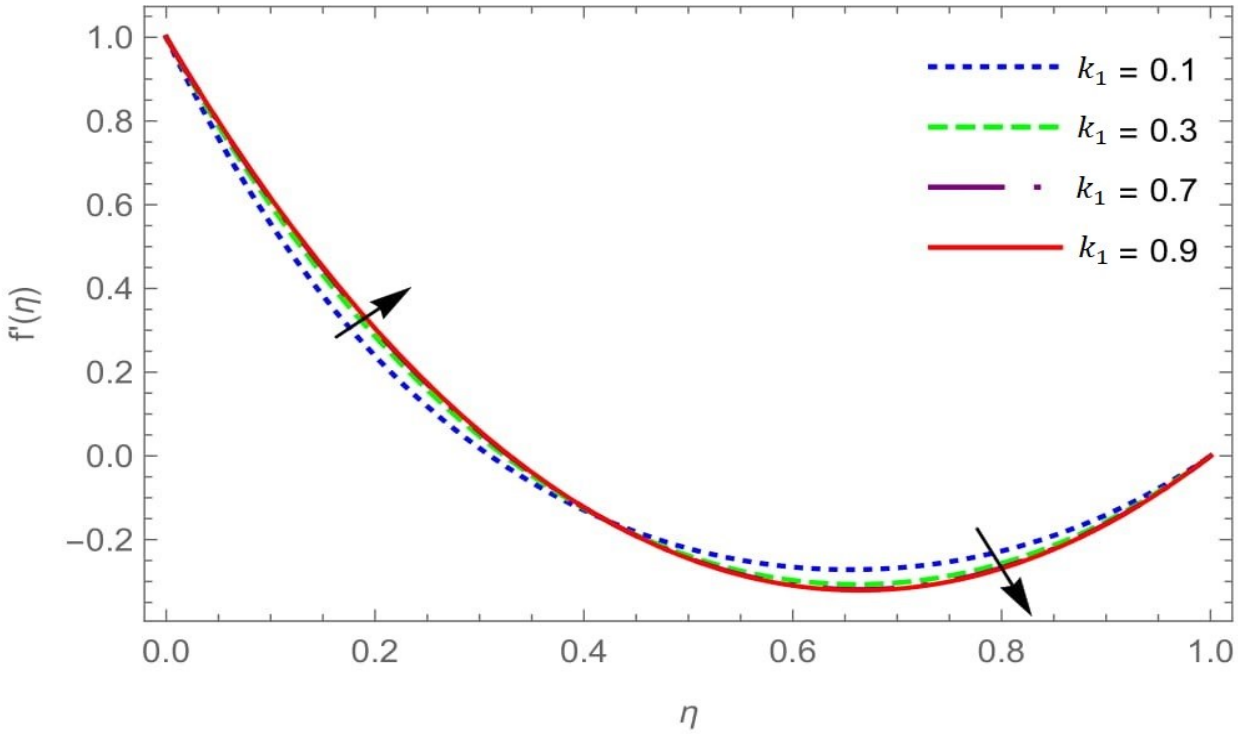

Figure 7.7: $\boldsymbol{f'(\eta)}$ for different values of $\boldsymbol{k_1}$.

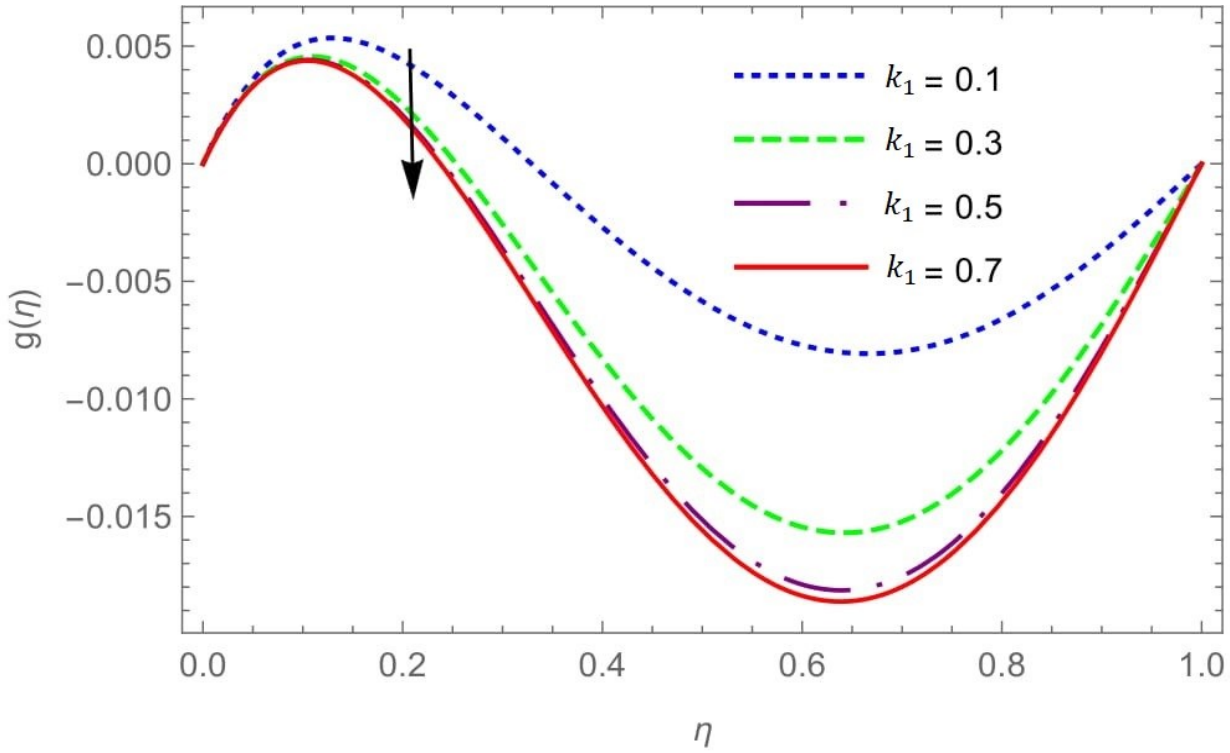

Figure 7.8: $\boldsymbol{g(\eta)}$ for different values of $\boldsymbol{k_1}$.

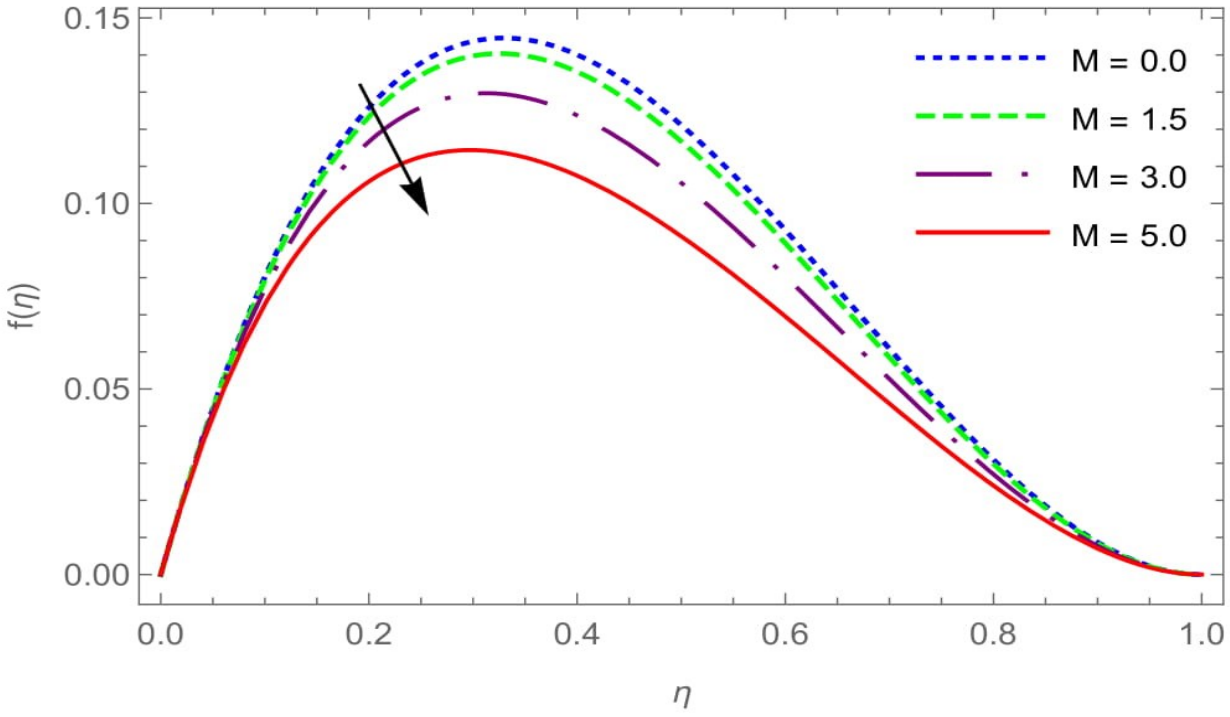

Figure 7.9: $\boldsymbol{f(\eta)}$ for different values of $\boldsymbol{M}$.

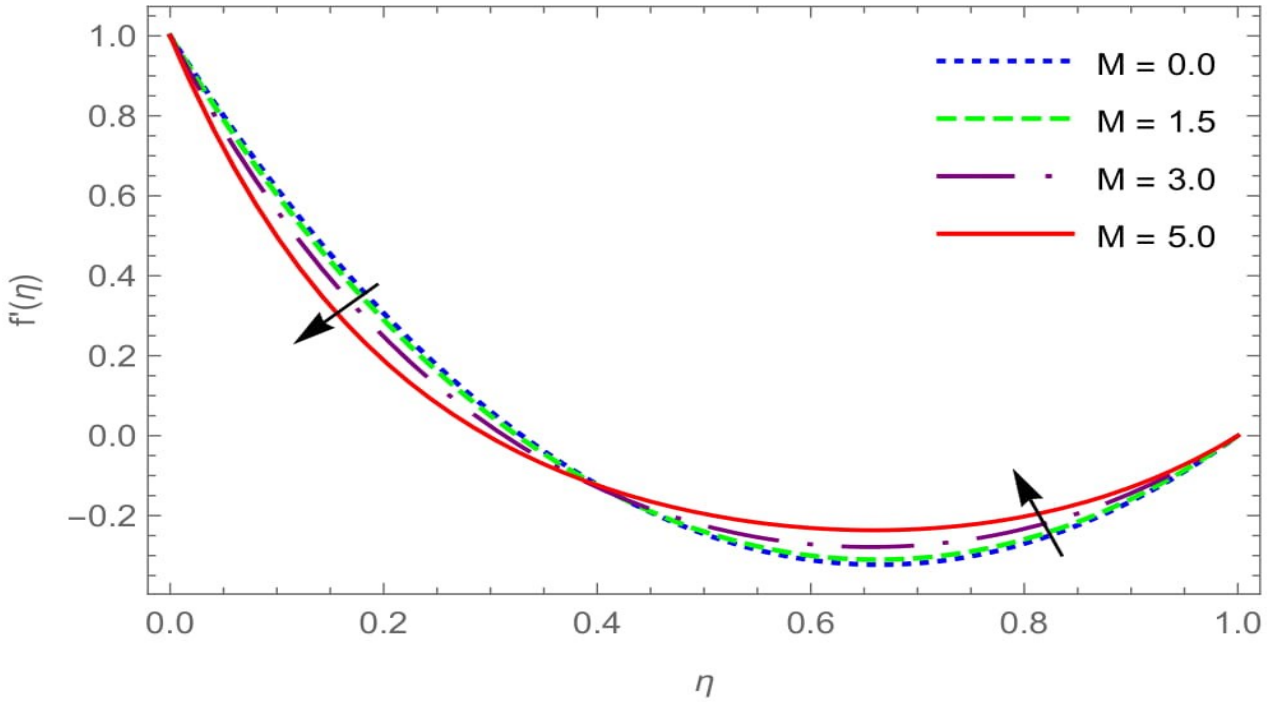

Figure 7.10: $\boldsymbol{f'(\eta)}$ for different values of $\boldsymbol{M}$.

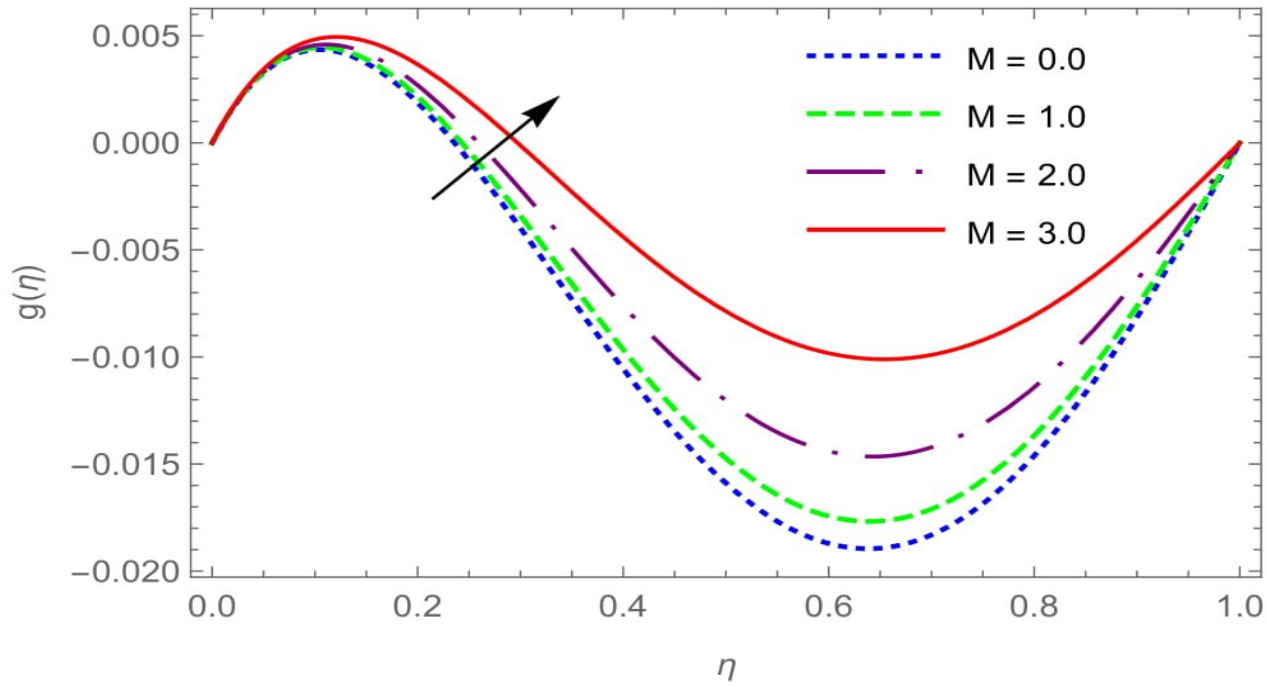

Figure 7.11: $\boldsymbol{g(\eta)}$ for different values of $\boldsymbol{M}$.

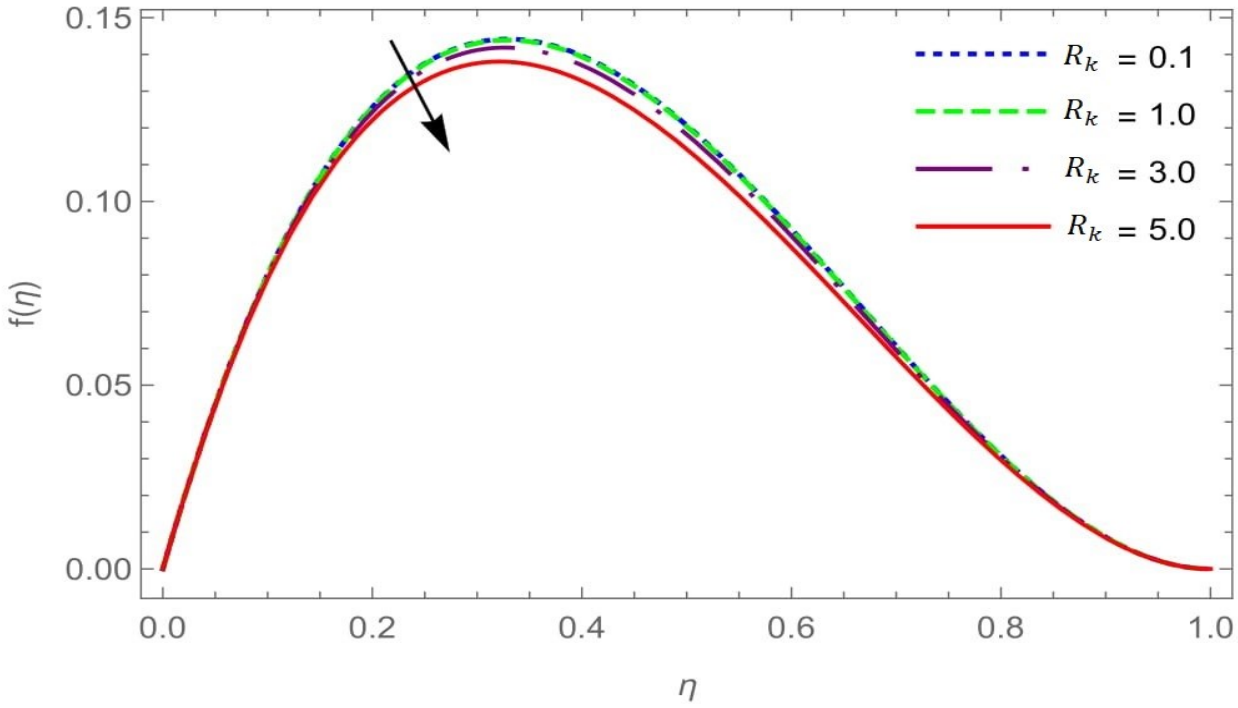

Figure 7.12: $\boldsymbol{f(\eta)}$ for different values of $\boldsymbol{Kr}$.

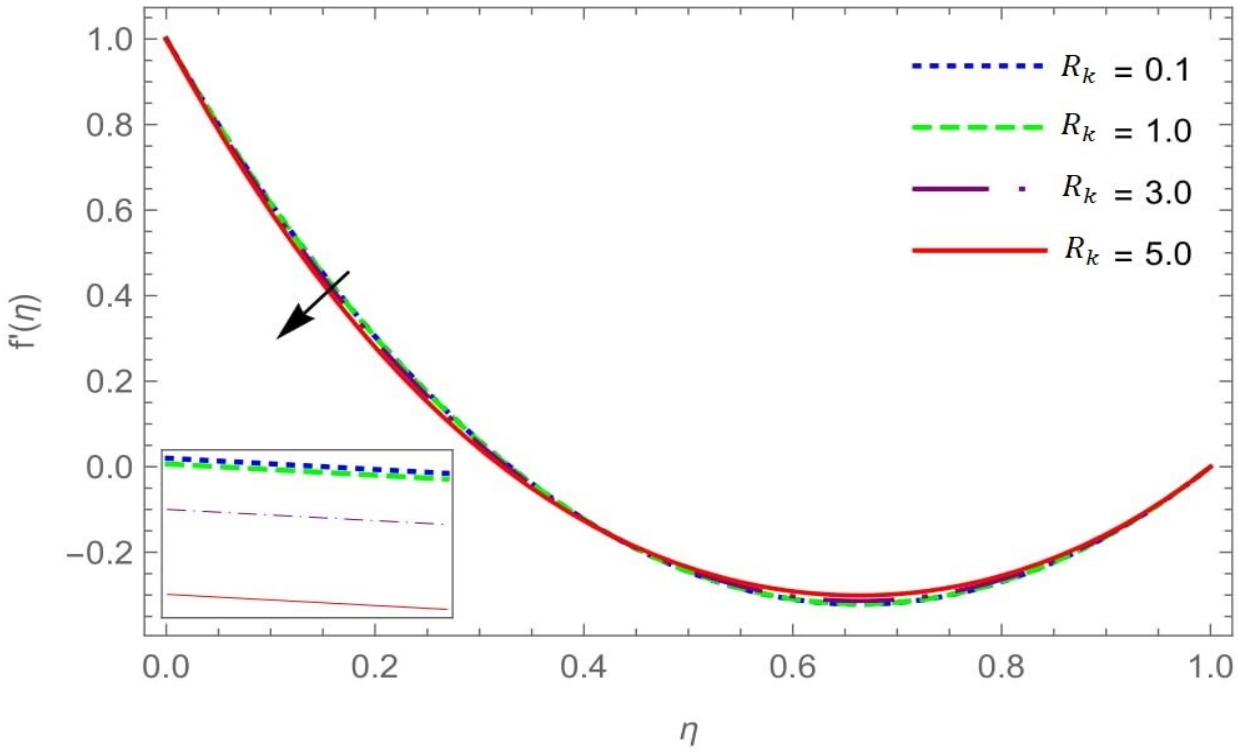

Figure 7.13: $\boldsymbol{f'(\eta)}$ for different values of $\boldsymbol{R_k}$.

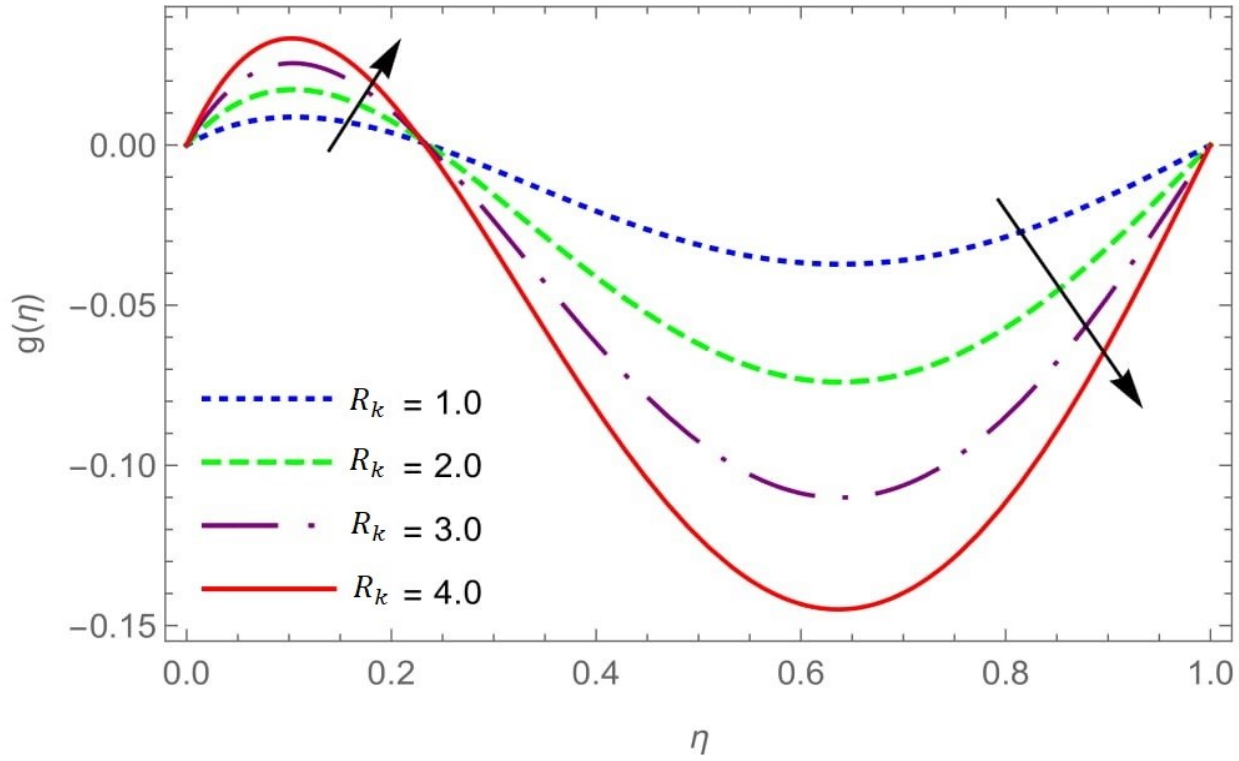

Figure 7.14: $\boldsymbol{g(\eta)}$ for different values of $\boldsymbol{R_k}$.

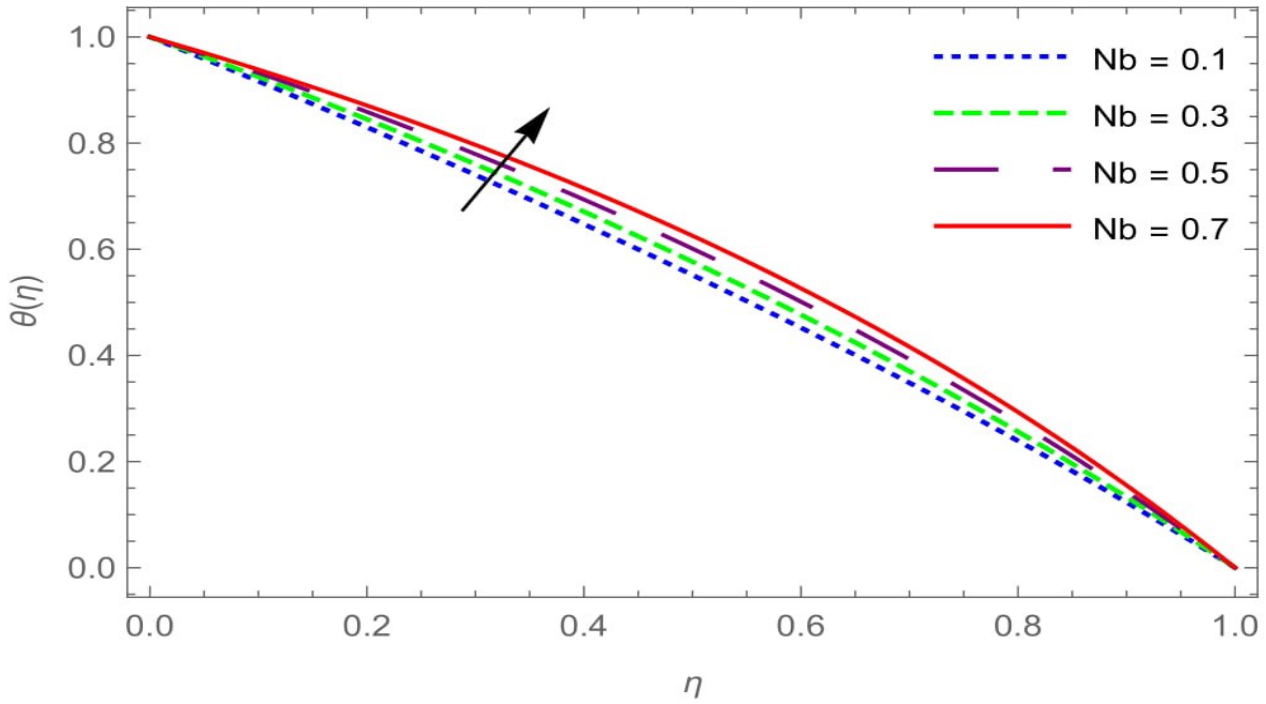

Figure 7.15: $\boldsymbol{\theta(\eta)}$ for different values of $\boldsymbol{Nb}$.

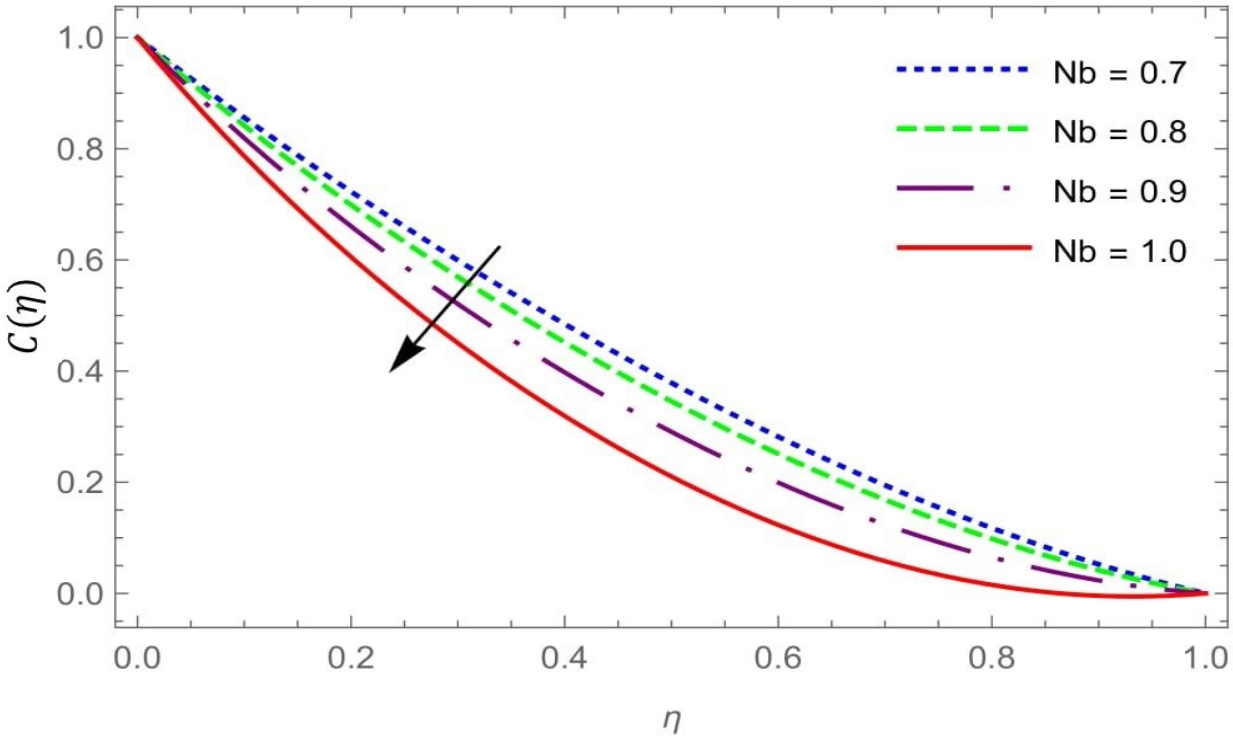

Figure 7.16: $\boldsymbol{C(\eta)}$ for different values of $\boldsymbol{Nb}$.

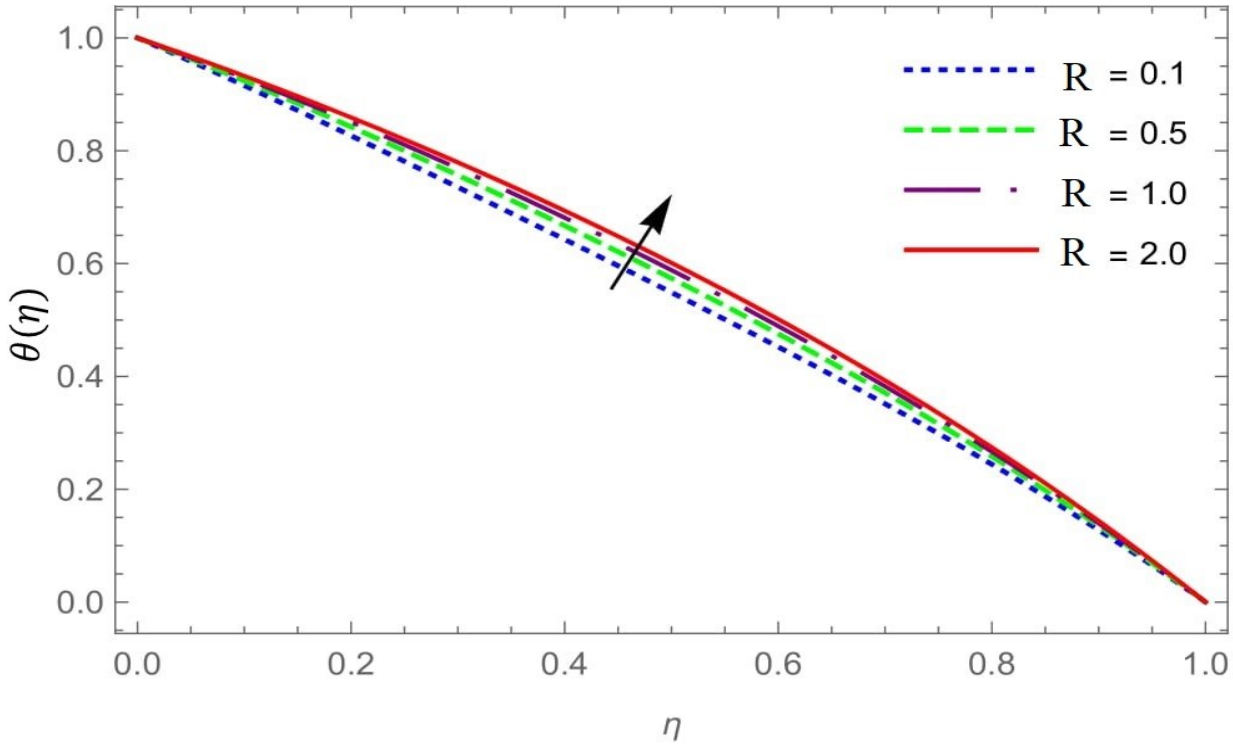

Figure 7.17: $\boldsymbol{\theta(\eta)}$ for different values of $\boldsymbol{R}$.

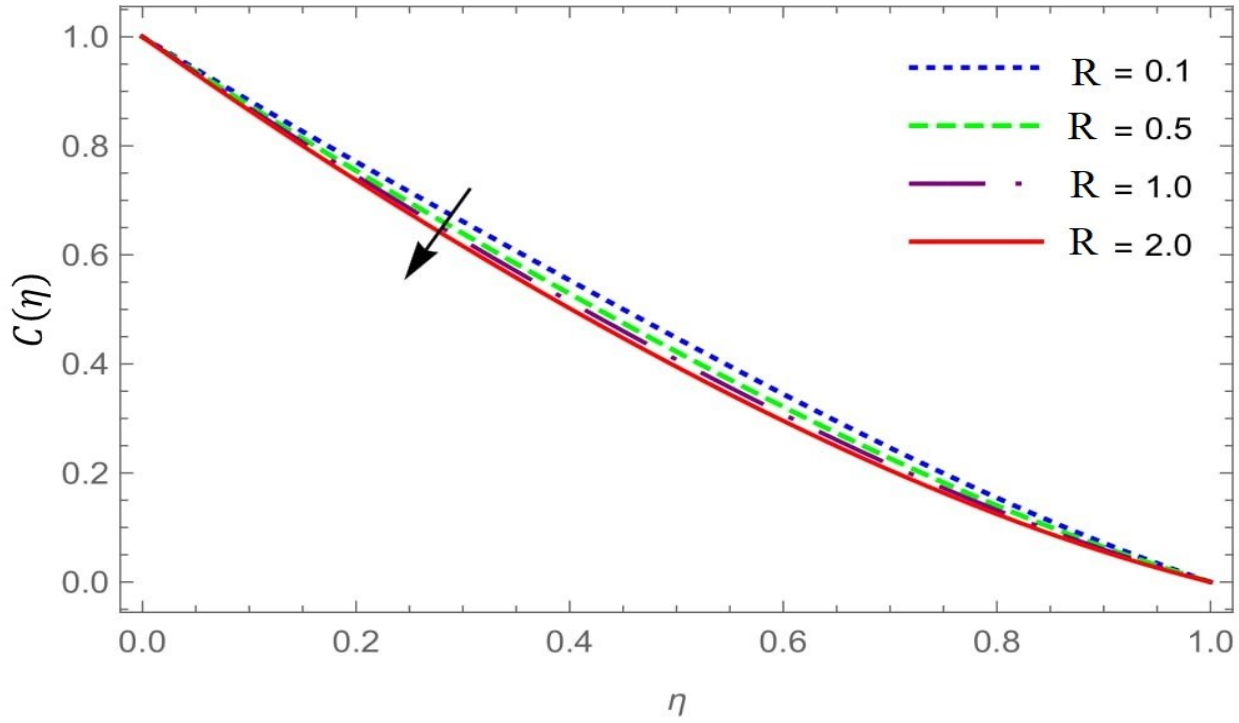

Figure 7.18: $\boldsymbol{C(\eta)}$ for different values of $\boldsymbol{R}$.

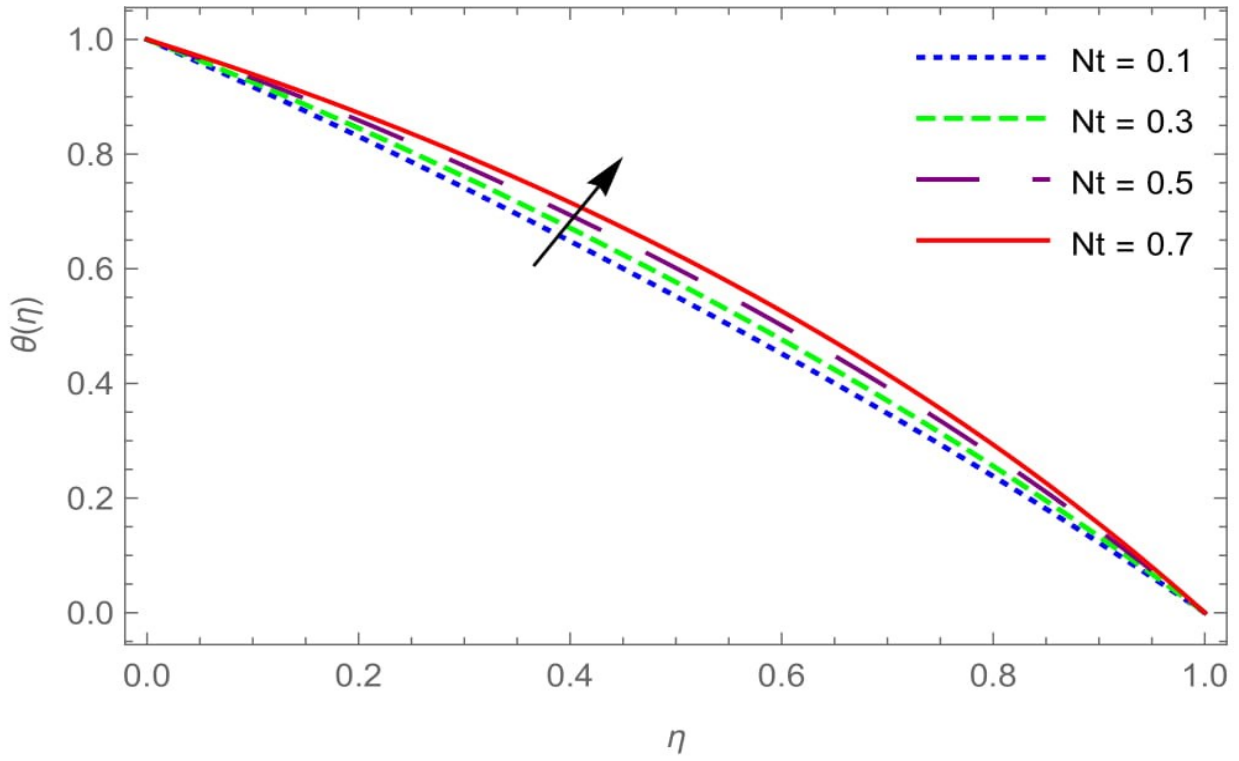

Figure 7.19: $\boldsymbol{\theta(\eta)}$ for different values of $\boldsymbol{Nt}$.

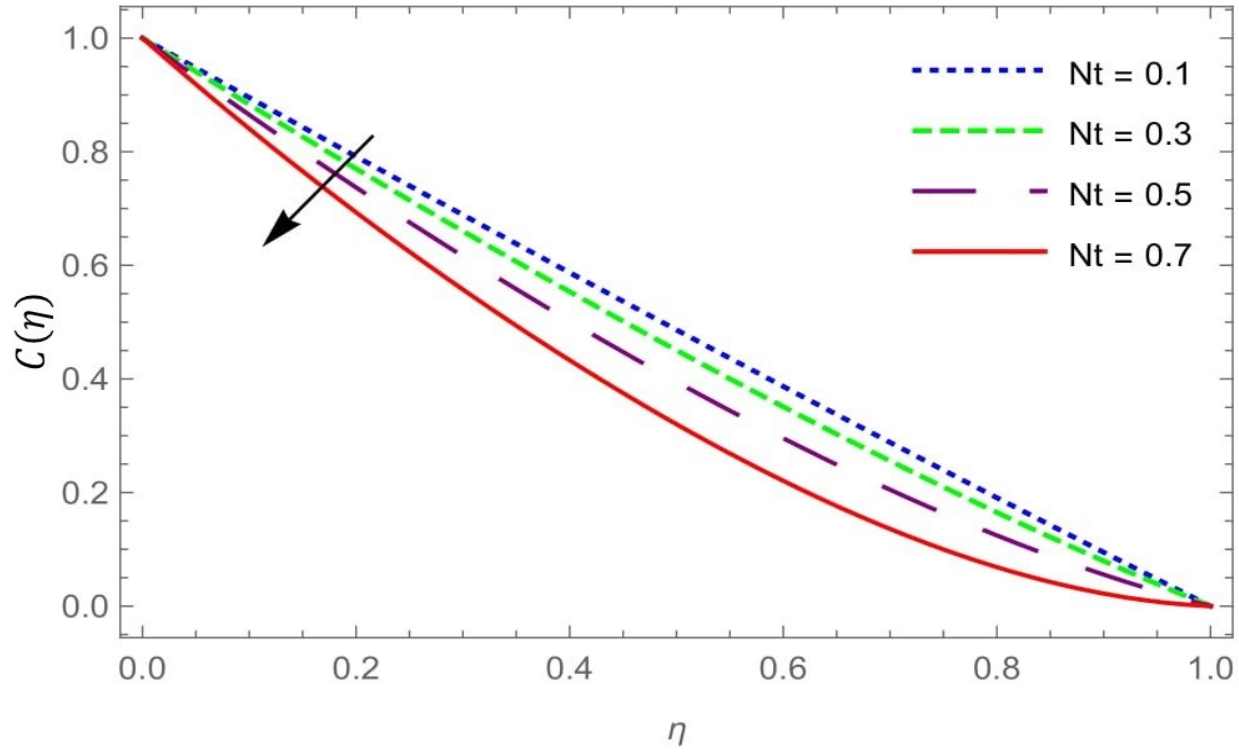

Figure 7.20: $\boldsymbol{C(\eta)}$ for different values of $\boldsymbol{Nt}$.

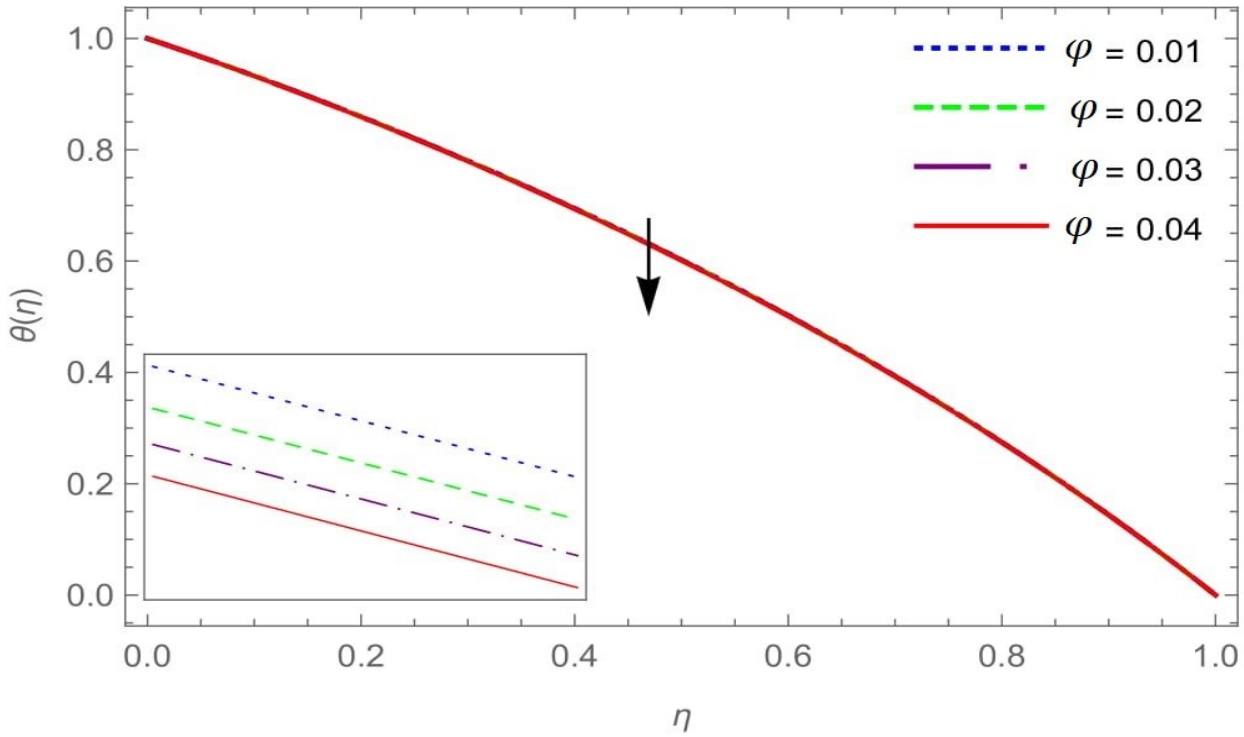

Figure 7.21: $\boldsymbol{\theta(\eta)}$ for different values of $\boldsymbol{\varphi}$.

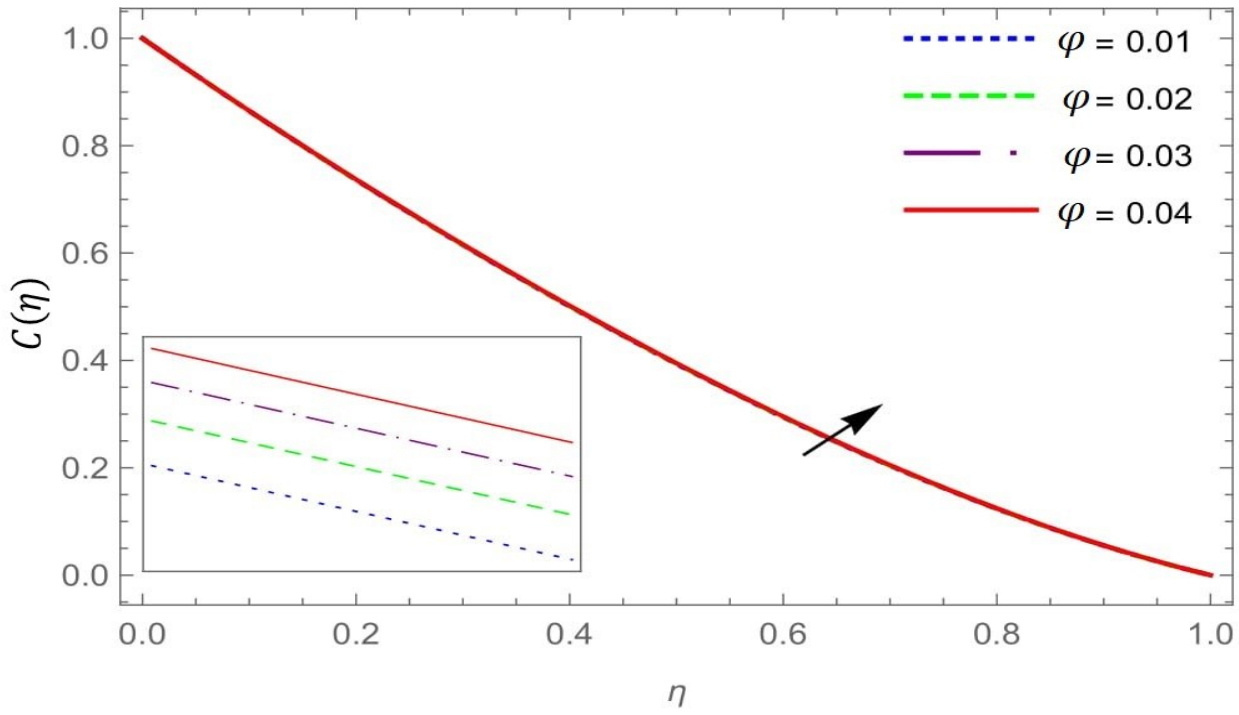

Figure 7.22: $\boldsymbol{C(\eta)}$ for different values of $\boldsymbol{\varphi}$.

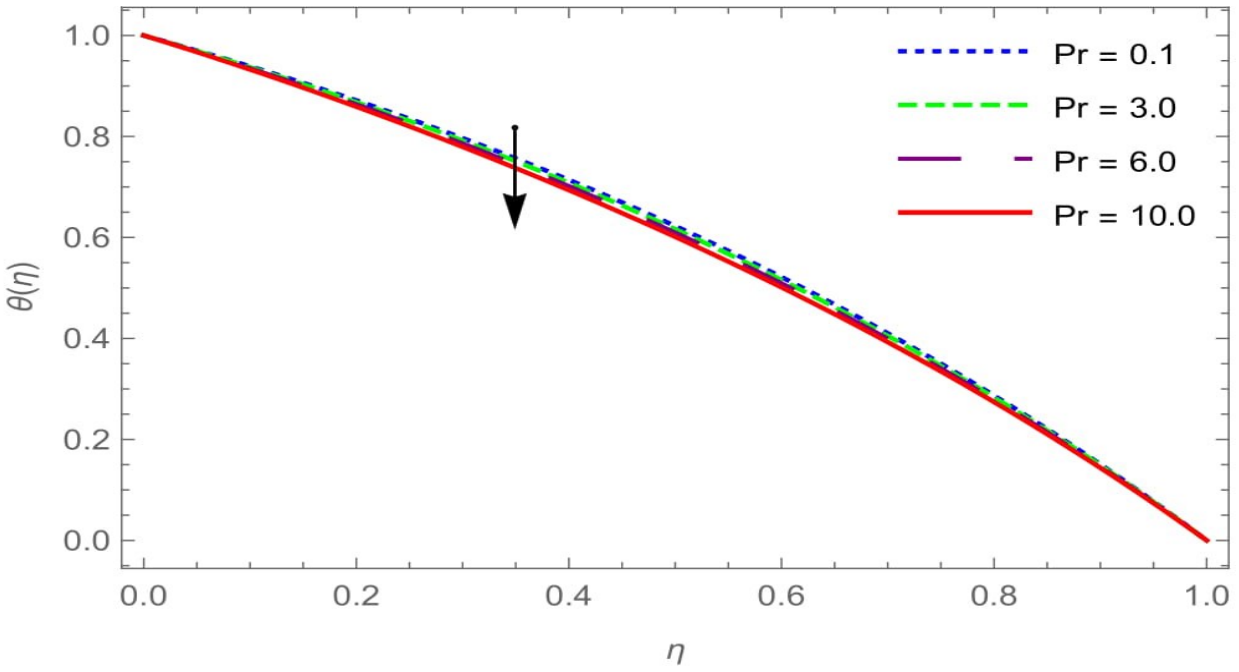

Figure 7.23: $\boldsymbol{\theta(\eta)}$ for different values of $\boldsymbol{Pr}$.

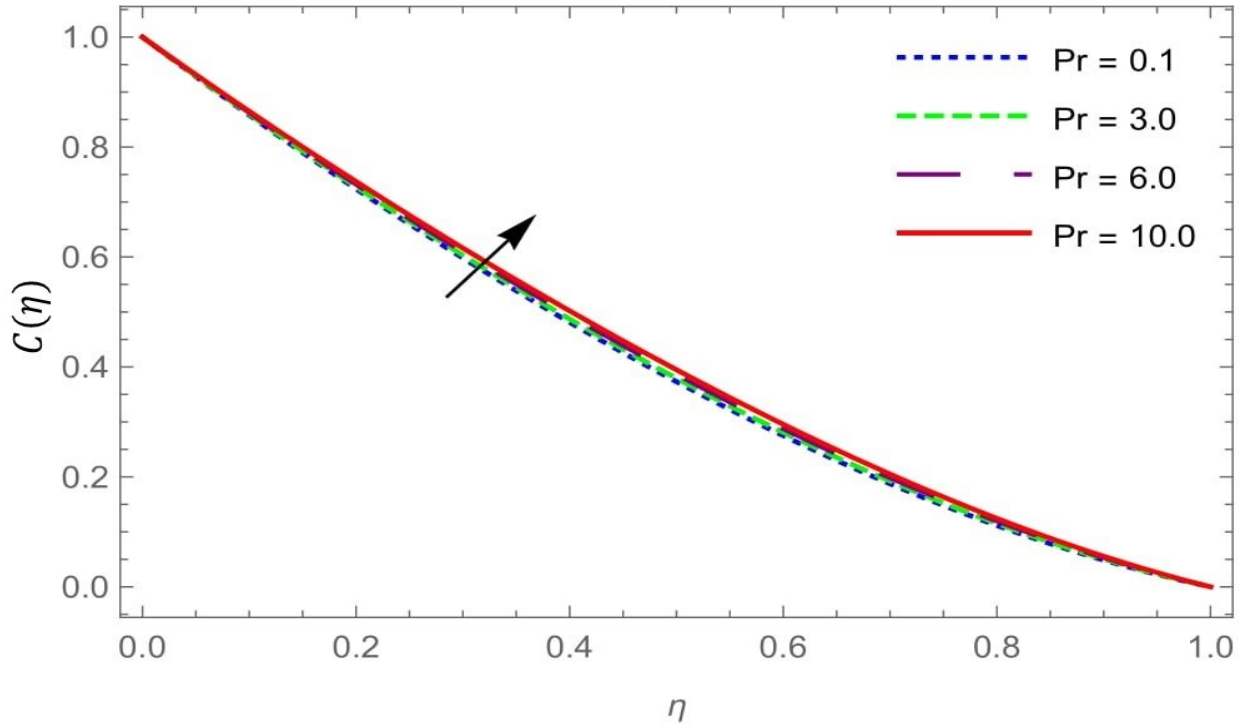

Figure 7.24: $\boldsymbol{C(\eta)}$ for different values of $\boldsymbol{Pr}$.

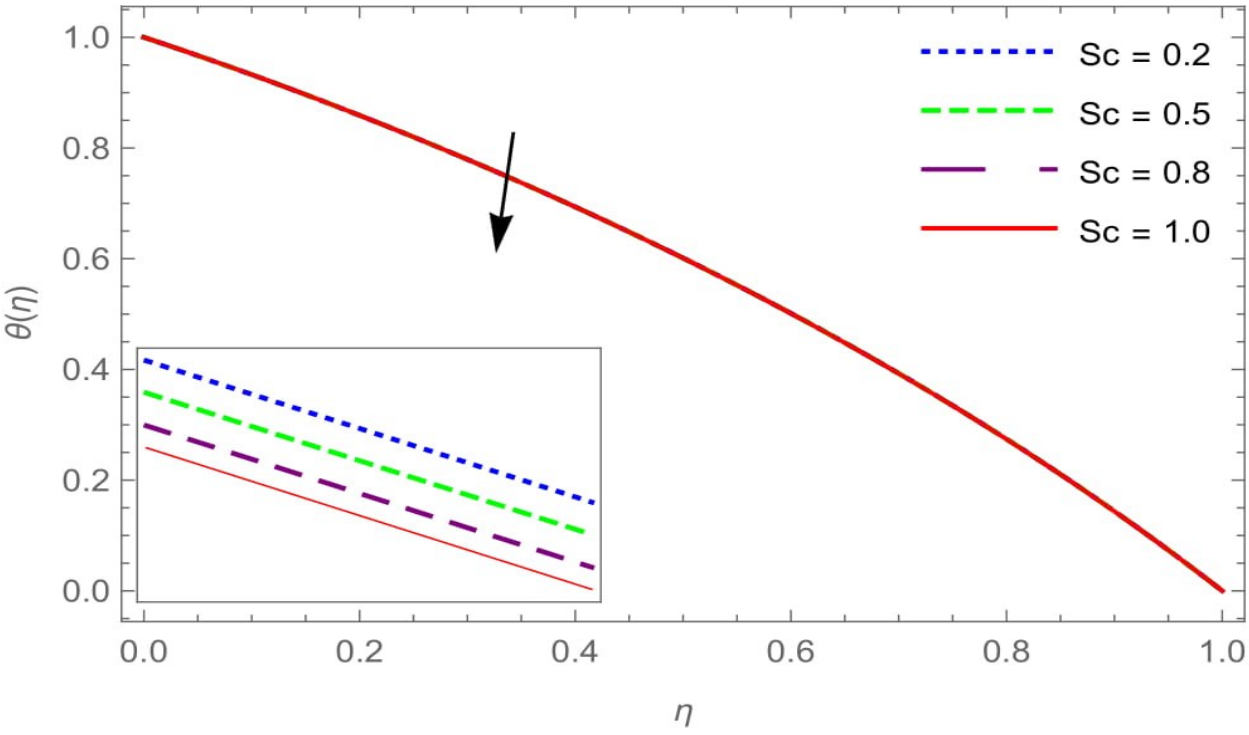

Figure 7.25: $\boldsymbol{\theta(\eta)}$ for different values of $\boldsymbol{Sc}$.

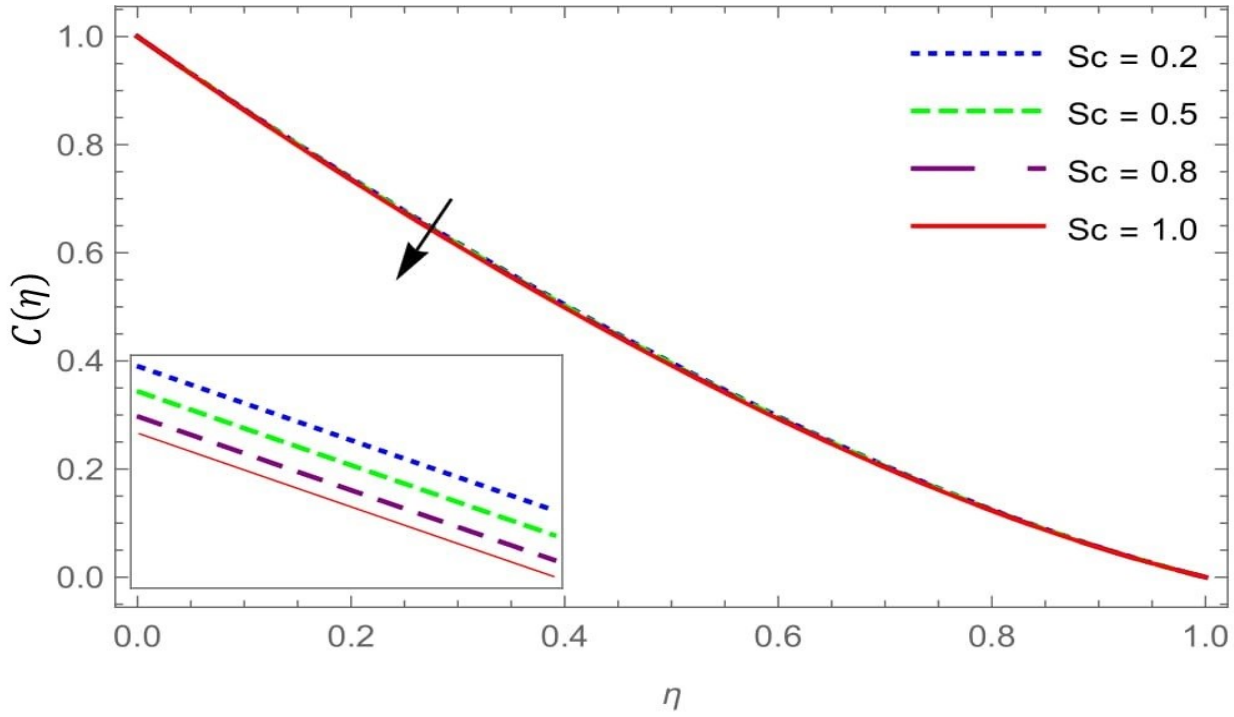

Figure 7.26: $\boldsymbol{C(\eta)}$ for different values of $\boldsymbol{Sc}$.

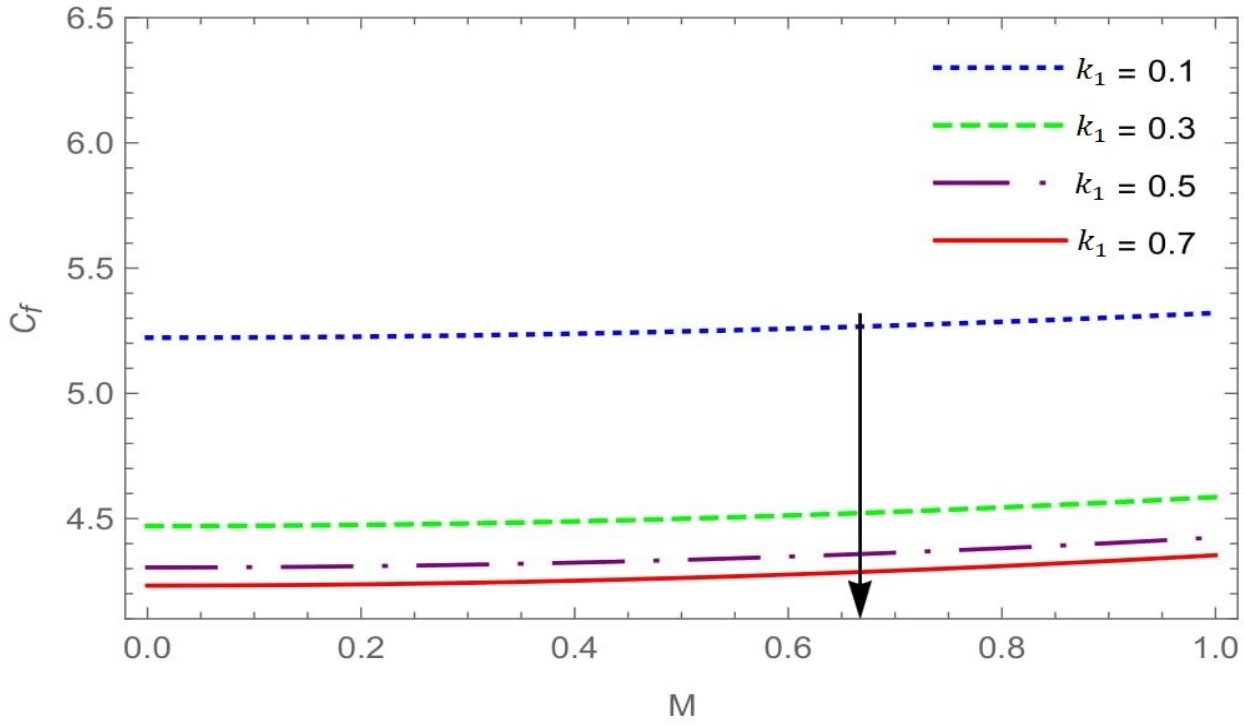

Figure 7.27: Skin Friction Coefficient $\boldsymbol{C_f}$ for different values of $\boldsymbol{k_1}$.

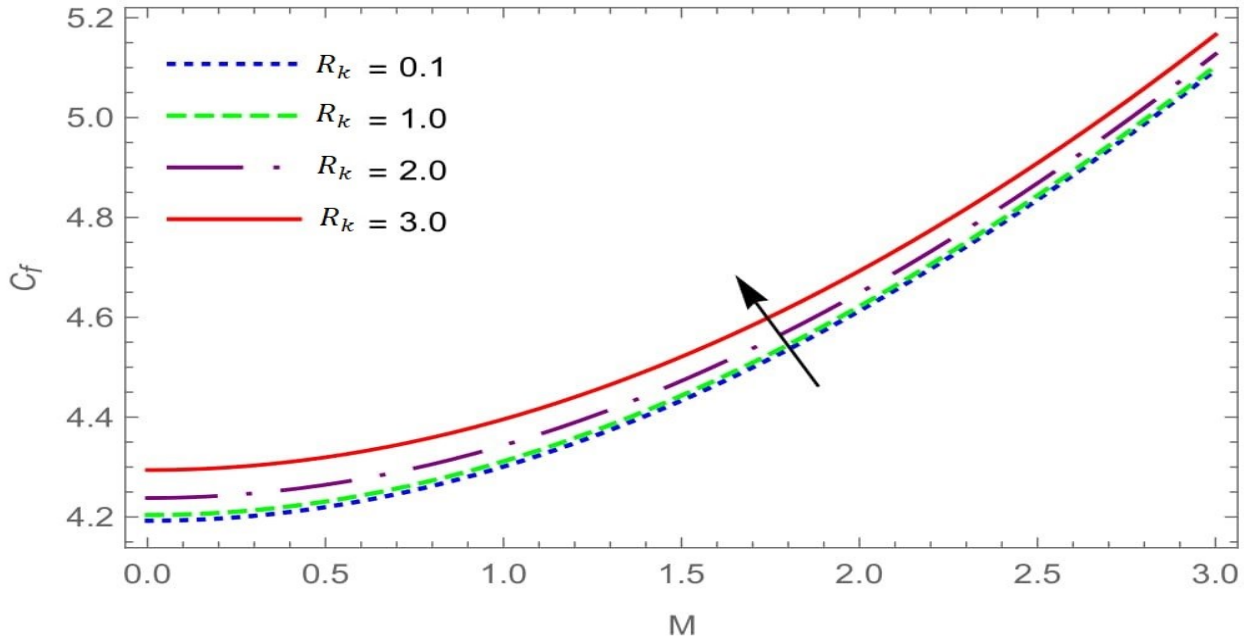

Figure 7.28: Skin Friction Coefficient $\boldsymbol{C_f}$ for different values of $\boldsymbol{R_k}$.

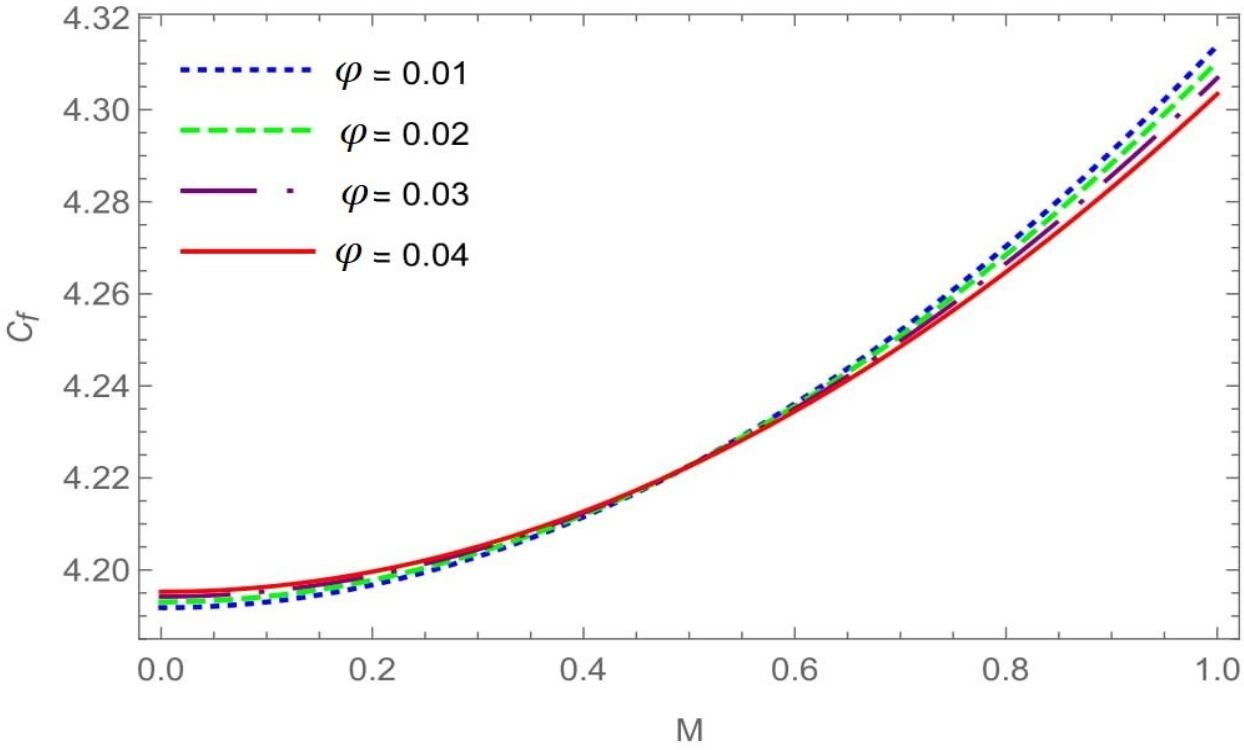

Figure 7.29: Skin Friction Coefficient $\boldsymbol{C_f}$ for different values of $\boldsymbol{\varphi}$.

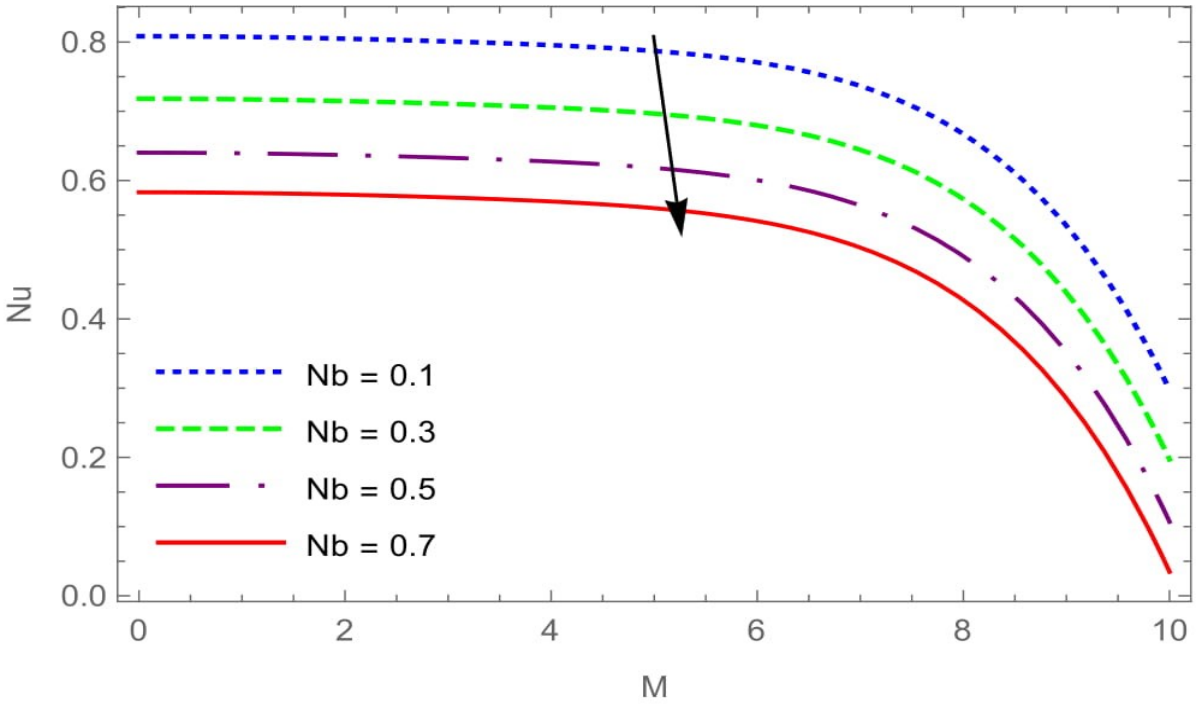

Figure 7.30: Nusselt Number variation $\boldsymbol{Nu}$ for different values of $\boldsymbol{Nb}$.

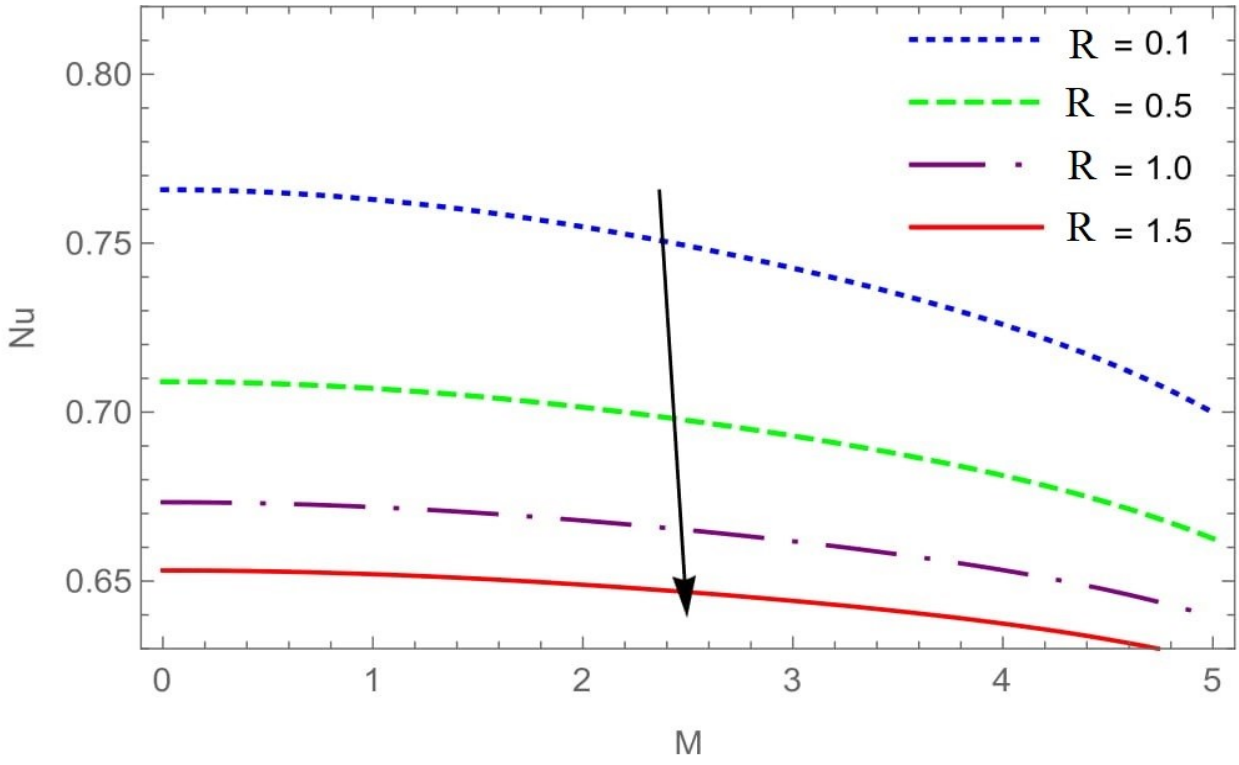

Figure 7.31: Nusselt Number variation $\boldsymbol{Nu}$ for different values of $\boldsymbol{R}$.

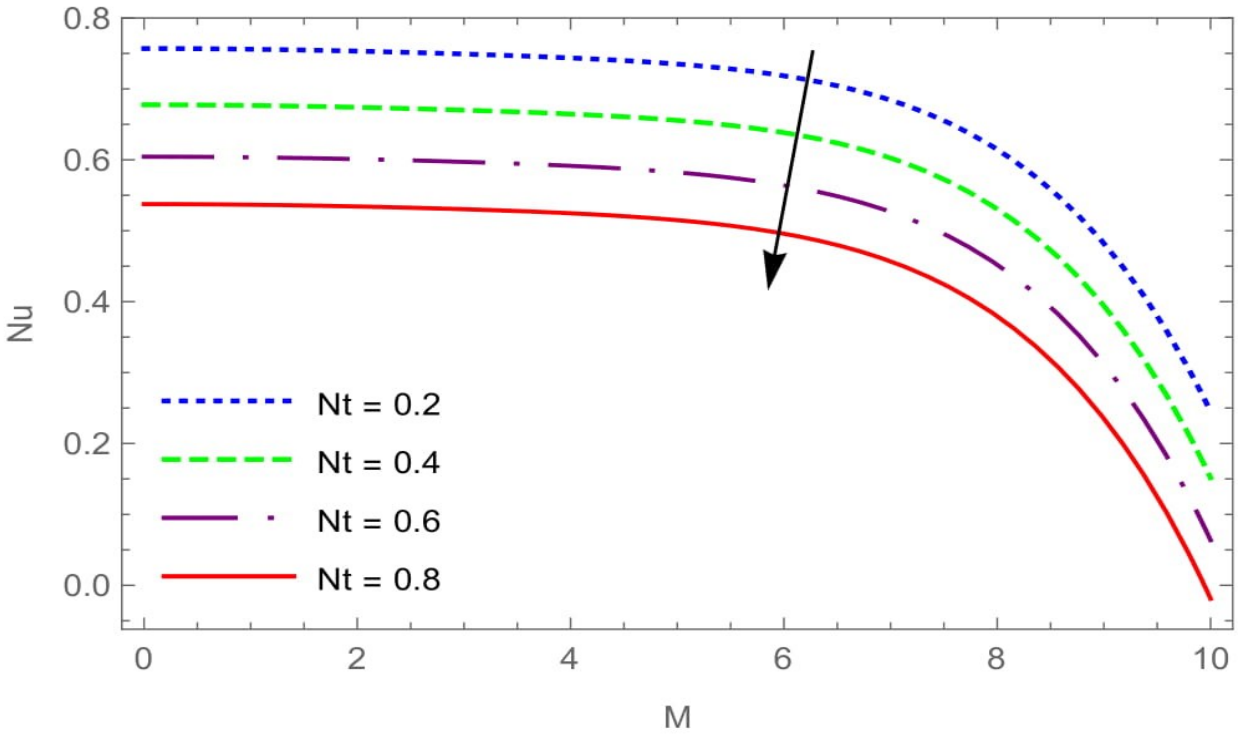

Figure 7.32: Nusselt Number variation $\boldsymbol{Nu}$ for different values of $\boldsymbol{Nt}$.

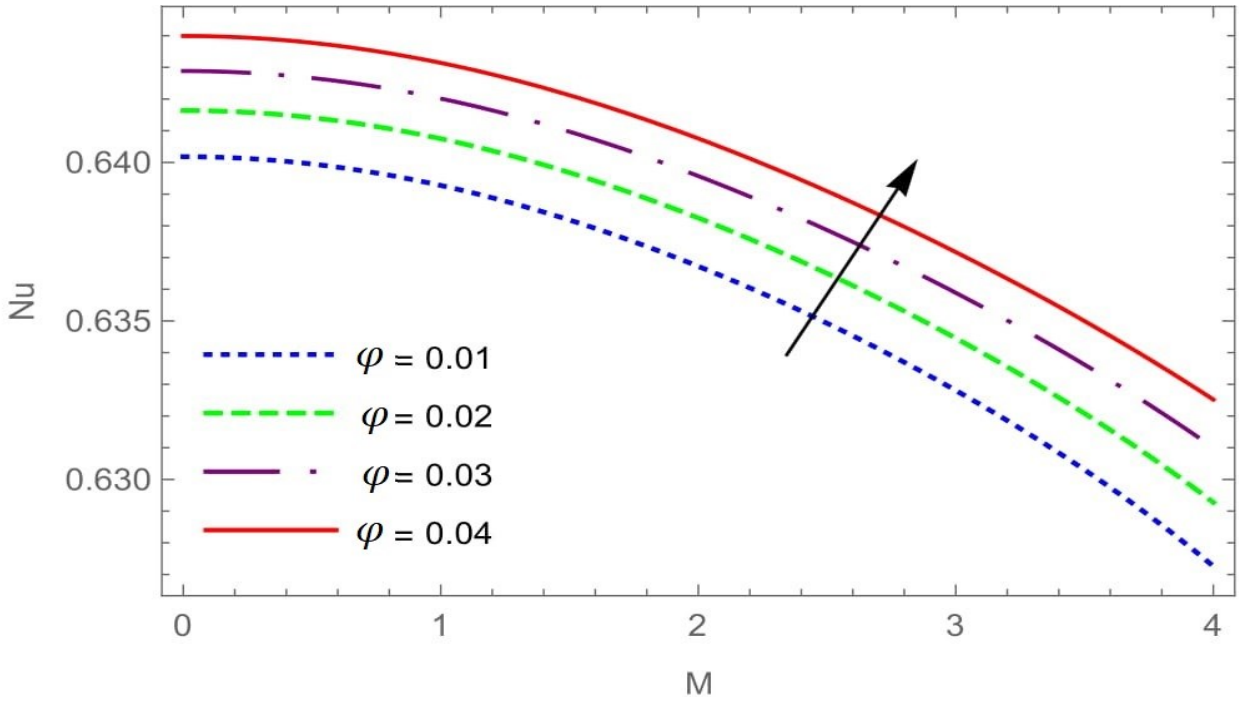

Figure 7.33: Nusselt Number variation $\boldsymbol{Nu}$ for different values of $\boldsymbol{\varphi}$.

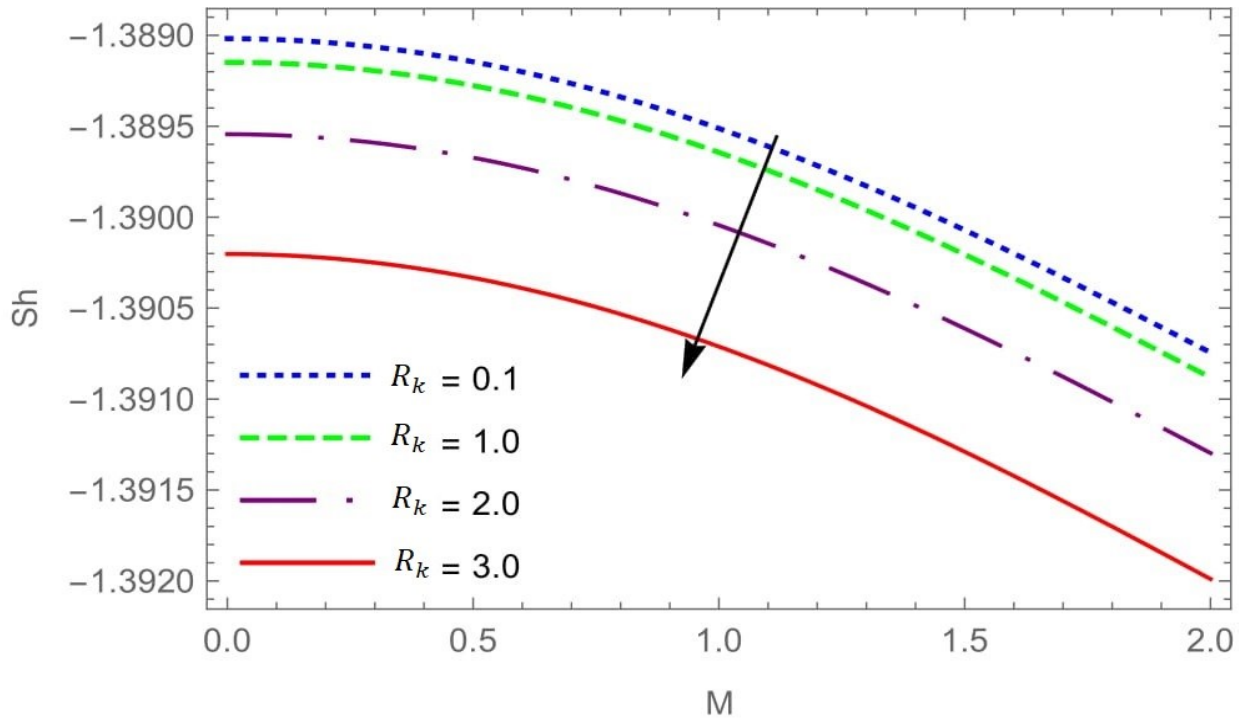

Figure 7.34: Sherwood Number variation $\boldsymbol{Sh}$ for different values of $\boldsymbol{R_k}$.

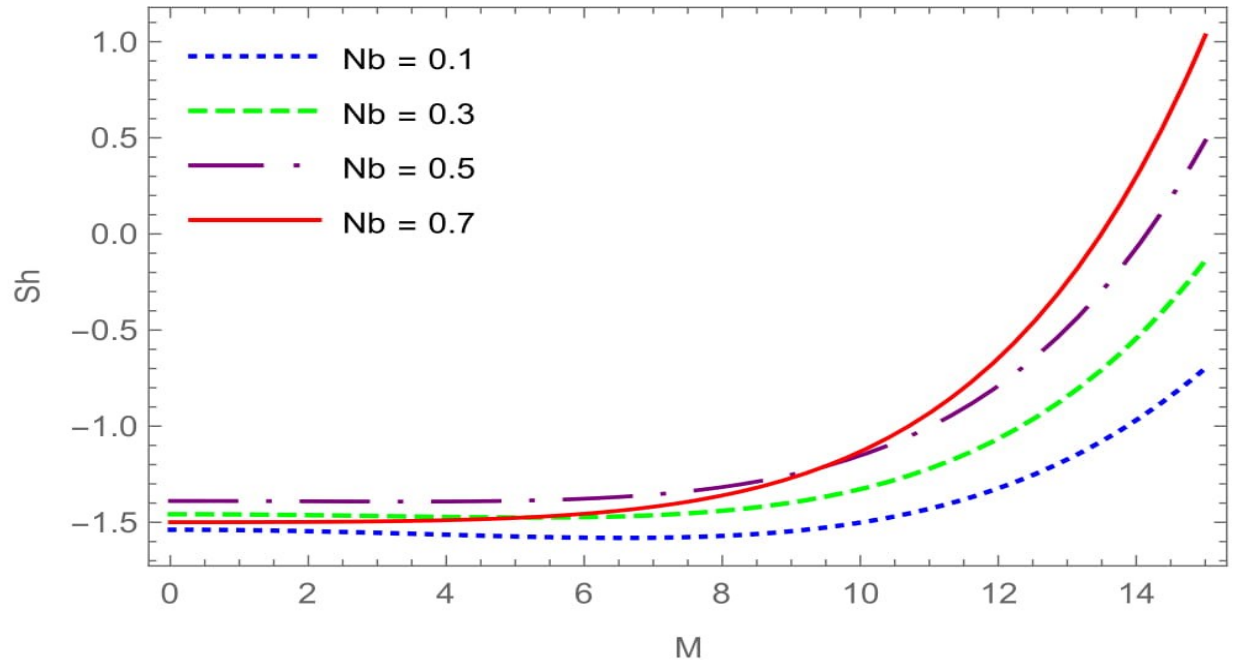

Figure 7.35: Sherwood Number variation $\boldsymbol{Sh}$ for different values of $\boldsymbol{Nb}$.

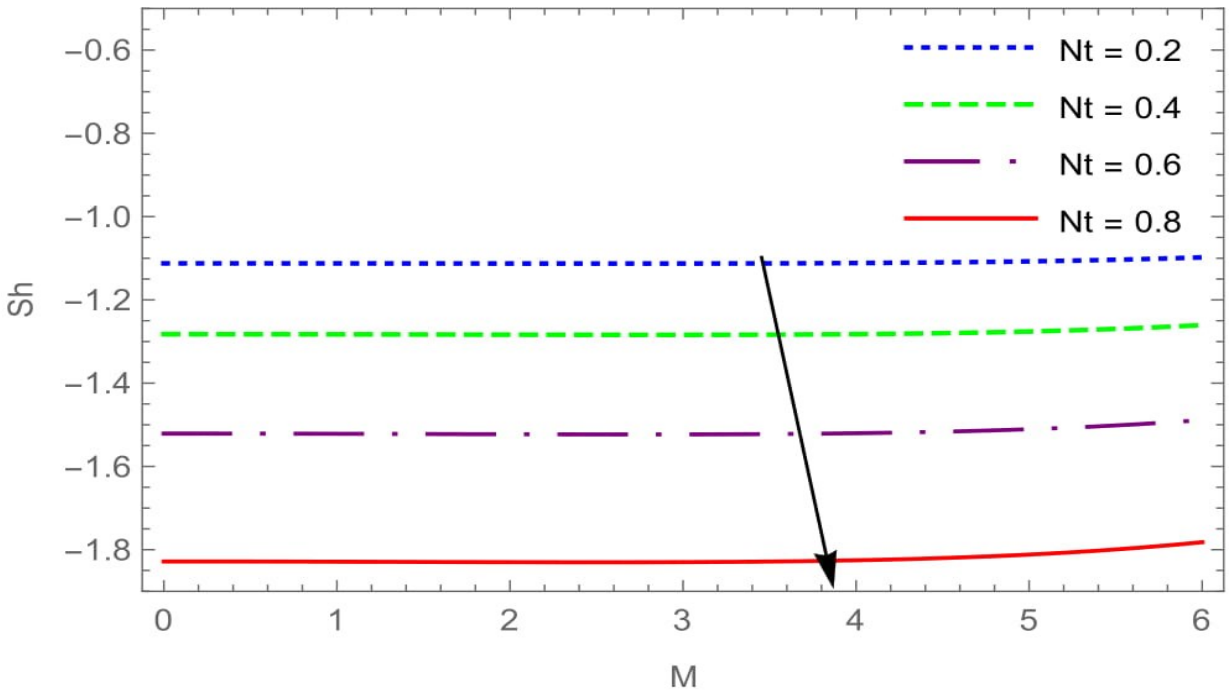

Figure 7.36: Sherwood Number variation $\boldsymbol{Sh}$ for different values of $\boldsymbol{Nt}$.

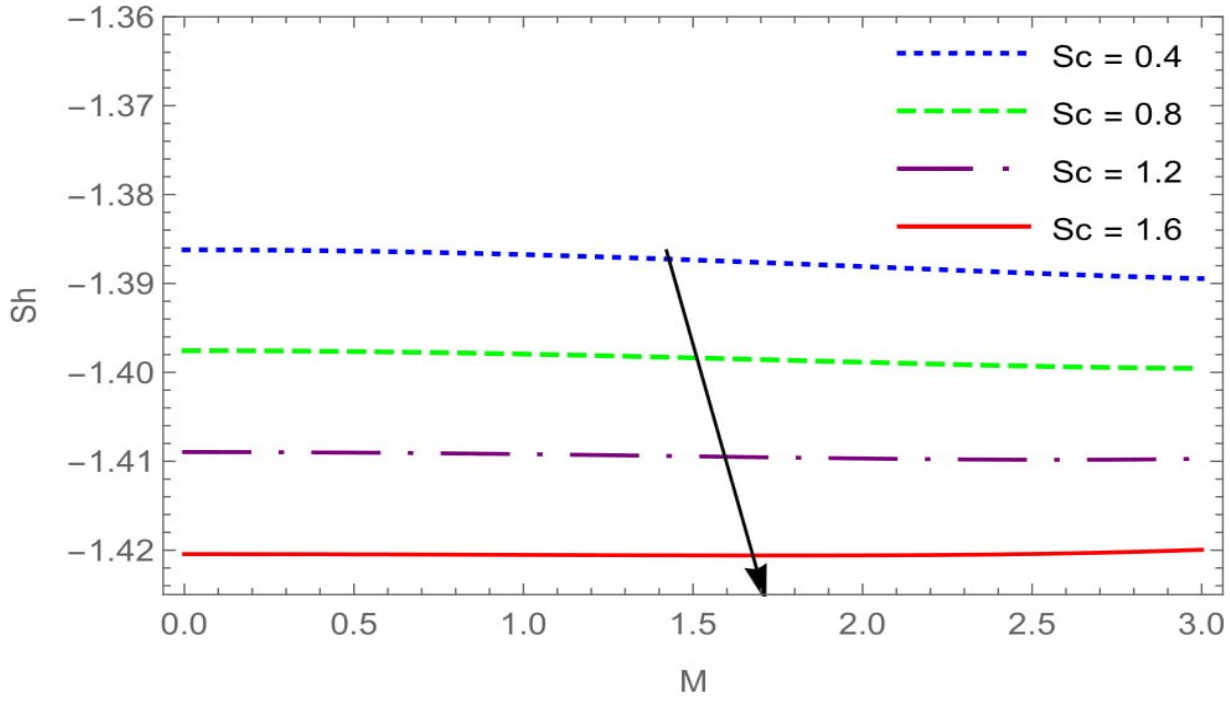

Figure 37: Sherwood Number variation $\boldsymbol{Sh}$ for different values of $\boldsymbol{Sc}$.

7.6 Conclusion:

The key remarks can be summarized as follows.

- Nanofluid velocity increases with decrease in magnetic parameter M.
- Nanofluid velocity escalates with k_1.
- Temperature of Nanofluid can be raised by raising anyone parameter from radiation, magnetic field, rotation, thermophoresis or Brownian.
- Nanofluid temperature decreases with rising values of $Sc\ or\ Pr$.
- Concentration increases by increasing φ or Pr.
- Concentration declines with increasing value of Thermophoresis parameter, Schmidt number and Brownian parameter.